Ionization Of Helium In A Non Coplanar Geometry

Timjan Kalajdzievski

A Thesis submitted to the Faculty of Graduate Studies in Partial Fulfillment of the Requirements for the Degree of Master of Science.

Graduate program in Physics and Astronomy, York University, Toronto, Ontario

August, 2016

Abstract

The purpose of this work is to calculate the scattering behaviour of a non-coplanar ionization collision of an electron with a helium atom. Relativistic distorted waves were used to describe the wave functions of the incident and scattered electron, and at large distances from the ionized atom the distorted waves for the outgoing electrons are a linear combination of relativistic coulomb waves. The T-matrix and scattering cross section were calculated with the assumptions that the incident electron impacted the atom perpendicularly to the scattering plane, defined by the trajectories of the two outgoing electrons which were assumed to have equal energies.

Acknowledgements

The author would like to thank Professor Al Stauffer for his thorough help and guidance throughout the work.

The author also expresses his gratitude to Mrs. Marlene Caplan for her quick and readily available assistance.

A special thanks is expressed to Professor Robert McEachran who provided some numerical results for the static potentials and bound states.

The author is grateful for his supportive family namely his parents Sasho Kalajdzievski and Nina Zorboski, and his siblings Darja and Damjan.

Lastly, the author would like to thank his fiancee Liz for her constant encouragement and love.

Contents

List of Figures

1 Introduction

Ionization collisions is a large subset of atomic physics where an incident particle with a particular energy, such as an electron, photon, positron etc. collides with a target atom and strips off an electron from the atom. This field is one that has been extensively researched and is studied experimentally by measuring the angles and energies of the outgoing electrons [1]. One of the earliest examples of an ionization collision experiment was in 1918, where an electron beam was directed at a solid metal cylinder, and led to the discovery of new lithium isotopes [2]. More modern experiments use a focused beam of electrons (focused to a single energy) which can impact target atoms propelled from a gas jet into the path of the electron gun [3], [4]. These gas jets are used in the case of noble gas targets, but targets can also include alkali-earth atoms, for example an atomic beam of magnesium produced from a heated oven [5]. This experiment also involved the use of a polarized laser to excite the magnesium atoms before the collision.

There are multiple methods to produce theoretical results in order to better understand the physics behind these experiments. These methods include time dependent perturba-

tions in the interaction picture, as well as calculating the T-matrix, and then the cross section, from relativistic or non relativistic solutions to the respective wave equations [6]-[10]. The cross section can also be calculated from the flux density, such as the work in [11] which uses a non relativistic approach for helium ionization with outgoing electrons of equal energy. Another recent paper used a method called the B-Spline R-Matrix approach as an application for electron atom collisions [12]. This B-Spline R-Matrix approach was used to solve for the radial scattering functions of the ionization. The theoretical results in this work are produced by calculating the T-matrix of the collision using relativistic methods and then calculating the triple differential cross section at varying outgoing angles and energies.

Many experiments in ionization collisions are in a co-planar geometry in which the incident particle is in the same plane as the outgoing particles, for example the paper by A. Dorn [8]. This paper examines an experiment where a beam of polarized electrons is used to ionize a xenon target. Recently, new experiments have been conducted on ionization collisions that have yet to be fully investigated (Murray et al. [3], [4]). More specifically, these are collisions for which the incoming electron is at an arbitrary angle

with respect to the scattering plane of the outgoing electrons, and the outgoing electrons are at equal energies. The experimental apparatus includes an electron gun and a gas jet mounted on a yoke which is rotated around the interaction region. Note that the incident electron beam is perpendicular to the atom beam from the gas jet, even when the angle of incidence is not 90 degrees. The target gas emits photons when excited by electron impact, and by observing the flux of these photons the electron beam is focused and steered onto the physical centre of rotation of the detectors and electron gun. The detectors are then tuned to measure electrons of equal energy, and in the perpendicular plane have an angular range of the measured cross section between 70 and 290 degrees from the axis of rotation of the electron gun. This range is dictated by the physical size of the detectors. [3], [4].

Theoretical papers have been published which calculate the T-matrix and compare the triple differential cross section to these non coplanar experimental results (e.g. [6] [7]). Due to the lower energies of these collisions, as well as the equal energy of the outgoing electrons, the interaction between the electrons must be taken into account [6]. In this work the post-collision interaction is approximated as a constant factor and taken out of

the integral calculations of the T-matrix. This constant factor allows the triple differential cross section to go to zero when the outgoing electrons are in the same position (separation angles of zero and one hundred eighty degrees). The constant factors that represent the post collision interaction of the electrons are called the Gamow and Ward-Macek factors [13]. These factors come from representing the post collision interaction with a coulomb function. The Gamow factor is the first two terms in this representation and involves the momenta of the outgoing electrons. The alternative Ward-Macek factor is the coulomb function evaluated at some average distance, and is the Gamow factor multiplied by the absolute value of a hypergeometric function. The Ward-Macek factor has a smaller effect then the Gamow factor on the overall normalization of the cross section [13].

The main purpose of this work is to use relativistic distorted waves in calculation of the T-Matrix in a non coplanar ionization collision, where the outgoing electrons have equal energy. I will observe the specific effects of the relativistic method on the total results in order to better understand their contribution. The ionization collision examined in this work will be for a He atom target. The calculations will be based on the framework provided by Tao Zuo [14], and all formula and results are presented in atomic units. I

will use wave functions that are solutions to the relativistic wave Dirac equation, as well as the Ward-Macek post-collision interaction factor to help produce results comparable to experiment.

2 Theory

The ionization process is completely represented by the calculation of the triple differential cross section, the exact form of this cross section given by:

$$\frac{d\sigma}{d\Omega_a d\Omega_b dE_a} = \frac{(2\pi)^4}{8}\frac{k_a k_b}{k_i}\sum_{s_i,s_a,s_b,m_b}|T|^2 \tag{1}$$

where the subscript a, b, and i correspond to the two outgoing electrons and the incident electron respectively. $d\Omega_a$ and $d\Omega_b$ are the solid angle elements, dE_a is the element of the final energy, and T is the T-matrix. The $(2\pi)^4$ normalization factor comes from the definition of the scattering amplitude [15]. The term involving the magnitudes of momentum k_a, k_b, and k_i are to allow the momenta in the incident and outgoing electrons have unit magnitude, which is a standard in the literature. The last normalization factor $\frac{1}{8}$ is due to averaging over the spin of the incident electron and the ejected electron, as well as the normalization of the wave function for the initial bound state.

In this work we are interested in the case where the energies of the two outgoing electrons are equal, so we have $E_a = E_b$. This gives one independent value of energy, since this

outgoing energy is also related to the energy of the incident electron. The geometry of the ionization is non-coplanar, meaning the incident electron is at a non zero angle with respect to the scattering plane which contains the scattered electrons. The two outgoing electrons are scattered at equal angles to the right and left of the projection of the incident electron on the scattering plane.

2.1 T-Matrix

The T-Matrix element T from equation (1), for an ionization collision is of the form:

$$T = \langle \Psi^{final} \Psi^{ion} | \, H_I \, | \Psi^{initial} \Psi^{atom} \rangle \tag{2}$$

With each Ψ being the respective wave functions and H_I as the interaction hamiltonian. The wave functions of the initial and two outgoing electrons will be described with relativistic distorted waves which account for the influence of the ion and atom on the electrons. At large distances the effect of the ion becomes a coulomb potential. A finite nucleus approximation is used as it allows for the correct behaviour of the bound state wave functions, and the coulomb waves in the final channel to depend on an integral power of r at the origin. A nucleus represented by a point charge would cause the integrals in this case to be divergent near the origin.

In the relativistic Dirac picture, the Hamiltonian for a system of two electrons can be written as

$$H = c\vec{\alpha} \cdot \vec{p}_1 + \beta c^2 - \frac{Z}{r_1} + c\vec{\alpha} \cdot \vec{p}_2 + \beta c^2 - \frac{Z}{r_2} + \frac{1}{r_{12}} \tag{3}$$

with r and p being position and momentum operators for each electron, and $\vec{\alpha}$ and β the standard Dirac matrices [16]. The leading term in the interaction part of this hamiltonian is then $\frac{1}{r_{12}}$ where the operator r_{12} is the relative position between the two electrons, or $r_{12} = |\vec{r}_1 - \vec{r}_2|$. Note that for a helium target there is also a third electron that remains bound to the nucleus after the collision, and is taken into account in the wave functions and static potentials of the atom and ion.

The spin flip effects in the relativistic picture allow the possibility of either one or both of the electrons involved in the ionization to have opposite spin after the collision. Due to spin flip the only good quantum number is the total angular momentum. The indistinguishability of two electrons prevents us from realizing some specific cases were the outgoing electrons have the same spin, or have spin different from their pre-collision states. These cases are called exchange and are subtracted from the direct elements due to antisymmetric wave functions.

The T-matrix that is calculated in the case of exchange will be referred to as the exchange part of the T-matrix, and similarly for the direct case. The direct and exchange

parts of the T-Matrix can then be written as

$$T^d = \langle F^{DWC-}_{b,s_1}(\vec{r}_1, s_1) F^{DWC-}_{a,s_2}(\vec{r}_2, s_2) He^+(\vec{r}_3, s_3)| \frac{1}{r_{12}} |F^{DW+}_{i,s_1}(\vec{r}_1, s_1) He(2,3)\rangle \qquad (4)$$

$$T^e = \langle F^{DWC-}_{b,s_2}(\vec{r}_1, s_2) F^{DWC-}_{a,s_1}(\vec{r}_2, s_1) He^+(\vec{r}_3, s_3)| \frac{1}{r_{12}} |F^{DW+}_{i,s_2}(\vec{r}_1, s_2) He(2,3)\rangle \qquad (5)$$

where the subscripts 1, 2, 3 refer to the three electrons in our system. More specifically these are the free electron in the incident channel, the electron that is ejected upon ionization, and the bound electron. We have also neglected the exchange of the free electron in the initial channel and the bound electron in the final channel, and have no change in the wave function of the helium atom between the direct and exchange elements. So in equation (1), the equation for the cross section, the "T" that represents the T-matrix will actually be the difference of these terms when the outgoing electrons have the same spins, and when the outgoing electrons have different spins the T-matrix will be either the direct or the exchange term depending on which spin channel is detected. The two outgoing electrons having the same spin makes them indistinguishable and then the cross section is proportional to the square of the difference of the direct and exchange T-matrix

terms.

From reference [14], the distorted wave in the incident channel is given by

$$F^{DW+}_{ch,\mu} = \frac{1}{(2\pi)^{3/2}} \frac{1}{kr} \sum_{\kappa m} e^{i\eta_k} a^{\mu}_{\kappa m} \left(\hat{\vec{k}_i}\right) \begin{pmatrix} f_\kappa \chi_{\kappa m} \\ \\ i g_\kappa \chi_{-\kappa m} \end{pmatrix} \tag{6}$$

and the distorted waves in the final channel following [7] (which are equivalent to [14]) is given by

$$F^{DWC-}_{ch,\mu} = \frac{1}{(2\pi)^{3/2}} \frac{1}{kr} \sum_{\kappa m} e^{-i\delta^c_k} a^{\mu}_{\kappa m} \left(\hat{\vec{k}_f}\right) \begin{pmatrix} y_1(kr) \chi_{\kappa m} \\ \\ i y_2(kr) \chi_{-\kappa m} \end{pmatrix} \tag{7}$$

with phase shifts η_k in the initial channel, δ^c_k in the final channel, and with

$$a^{\mu}_{\kappa m}\left(\hat{\vec{k}}\right) = 4\pi i^l \sqrt{\frac{E + c^2}{2E}} \sum_{m_l} (l m_l \frac{1}{2} \mu | J m) Y^*_{l m_l}\left(\hat{\vec{k}}\right) \tag{8}$$

where E is the total energy including rest mass of the incident electron and μ is the spin component. The term multiplied by the spherical harmonic in the sum is a standard Clebsch-Gordan coefficient, and is given an explicit form in equation (16) on page 22. The functions in equations (6) and (7) denoted by f_κ, g_κ and $y_1(kr)$, $y_2(kr)$ are the regular

and irregular component wave functions of the incident and final channels respectively.

The spin angular functions $\chi_{\pm\kappa m}$ are given by

$$\chi_{\kappa m}\left(\hat{\vec{r}},\sigma\right) = \sum_{m_l,\mu}(lm_l\frac{1}{2}\mu|Jm)Y_{l,m_l}\left(\hat{\vec{r}}\right)\Psi_{1/2,\mu}(\sigma) \tag{9}$$

and

$$\chi_{-\kappa m}\left(\hat{\vec{r}},\sigma\right) = \sum_{\bar{m}_l,\mu}(\bar{l}\bar{m}_l\frac{1}{2}\mu|Jm)Y_{\bar{l},\bar{m}_l}\left(\hat{\vec{r}}\right)\Psi_{1/2,\mu}(\sigma) \tag{10}$$

with $\bar{l} = l - s_\kappa$ and $s_\kappa = \frac{\kappa}{|\kappa|}$. The orbital angular momentum part given by $Y_{l,m_l}\left(\hat{\vec{r}}\right)$ which are the spherical harmonics, and with $\Psi_{1/2,\mu}(\sigma)$ being the spin component functions.

The spherical harmonics are given by

$$Y_{lm}(\theta,\phi) = \sqrt{\frac{2l+1}{4\pi}\frac{(l-m)!}{(l+m)!}}P_l^m(cos\theta)e^{im\phi} \tag{11}$$

with P_l^m the associated Legendre functions. Note that the spherical harmonics obey the relationship $Y_{l-m}(\theta,\phi) = (-1)^m Y_{lm}^*(\theta,\phi)$ since the Legendre functions are real. In the experiment of [4] the outgoing electrons are on opposite sides of the incident electron in the scattering plane. So for that case the first scattered electron has $\phi = 0$ and the second

has $\phi = \pi$ making the spherical harmonics real.

2.1.1 Radial And Angular Parts Of The T-Matrix

Using equations (6) to (10) we can expand the direct T-Matrix into radial and angular parts. The expanded inter electronic term in the T-Matrix is

$$\frac{1}{r_{12}} = \sum_{\lambda\mu} \frac{r_<^\lambda}{r_>^{\lambda+1}} \frac{4\pi}{2\lambda+1} Y^*_{\lambda\mu}(1) Y_{\lambda\mu}(2) = \sum_{\lambda\mu} \frac{r_<^\lambda}{r_>^{\lambda+1}} C^*_{\lambda\mu}(1) C_{\lambda\mu}(2) \tag{12}$$

where $r_<$ and $r_>$ are the smaller and larger of the radii respectively. So the expanded radial part of the direct T-Matrix is

$$\begin{aligned} T_R = \int_0^\infty \Big(& \frac{1}{r_2^{\lambda+1}} \int_0^{r_2} \left[y_1^a(r_1) P_{1s}(r_1) + y_2^a(r_2) Q_{1s}(r_2) \right] r_1^\lambda dr_1 \\ & + r_2^\lambda \int_{r_2}^\infty \left[y_1^a(r_1) P_{1s}(r_1) + y_2^a(r_2) Q_{1s}(r_2) \right] \frac{dr_1}{r_1^{\lambda+1}} \Big) \left[y_1^b(r_2) f_k(r_2) + y_2^b(r_2) g_k(r_2) \right] dr_2 \end{aligned} \tag{13}$$

with $P_{1s}(r)$ and $Q_{1s}(r)$ the bound state orbitals of the helium atom. Note that for $r > r_N$ the bound state orbitals are zero (Where r_N is defined as the radius at which this takes place). In this region the inner integrals will behave as $\frac{1}{r^{\lambda+1}}$ and zero. For $r_2 > r_N$ the total inner integral will have a simple form which can be evaluated using the asymptotic expansions gone over in section 2.2.5 and with more detail in the appendix.

Letting the radial part of the T-Matrix be represented by T_R, the full T-Matrix with the angular parts ($E_a = E_b$, $\hat{\vec{k}}_i$ fixed, and $s_i = 1/2$) is then

$$T_d(s_a, s_b, E_a, E_i) = \frac{(4\pi)^3}{(2\pi)^{9/2}} \frac{1}{k_i k_a^2} \left(\frac{E_a + c^2}{2E_a} \right) \sqrt{\frac{E_i + c^2}{2E_i}}$$

$$\times \sum_{\kappa_a m_a m_{la}} \sum_{\kappa_b m_b m_{lb}} \sum_{\kappa_i m_i m_{li}} \sum_{\lambda \rho} i^{(l_i - l_a - l_b)} e^{i(\delta^c_{k_a} + \delta^c_{k_b} + \eta_{k_a})}$$

$$\times (l_a m_{la} \frac{1}{2} s_a | j_a m_a) Y_{l_a m_{la}}(\hat{\vec{k}}_a)$$

$$\times (l_b m_{lb} \frac{1}{2} s_b | j_b m_b) Y_{l_b m_{lb}}(\hat{\vec{k}}_b)$$

$$\times (l_i m_{li} \frac{1}{2} s_i | j_i m_i) Y^*_{l_i m_{li}}(\hat{\vec{k}}_i)$$

$$\times d^\lambda_\rho(\kappa_i m_i, \kappa_b m_b) d^\lambda_\rho(\kappa_a m_a, 1 s m_{1s}) \times T_R \quad (14)$$

with $m_a = m_{la} + s_a$, $m_b = m_{lb} + s_b$, $m_i = m_{li} + s_i$, and where

$$d^\lambda_\rho(j' m', jm) = (-1)^{m+1/2} \sqrt{(2j+1)(2j'+1)} \begin{pmatrix} j & \lambda & j' \\ 1/2 & 0 & -1/2 \end{pmatrix} \begin{pmatrix} j & \lambda & j' \\ -m & \rho & m' \end{pmatrix} \quad (15)$$

Note that from the properties of the 3j symbols we have the parity condition that $l + \lambda + l'$ is even, and the value of $\rho = m_{1s} - m_a = m_b - m_i$. Also note that E_i is related

to E_a through the ionization energy. More specifically, the ionization energy added to E_i is equal to twice the value of E_a.

We can also write the Clebsch Gordan coefficients in terms of the 3j symbols with the relation

$$(lm_l\frac{1}{2}s|jm) = (-1)^{l-1/2+m}\sqrt{(2J+1)}\begin{pmatrix} l & 1/2 & j \\ m_l & s & -m \end{pmatrix} \tag{16}$$

Substituting equations (15) and (16) into equation (14) and simplifying gives

$$T_d(s_a, s_b, E_a, E_i) = \left(\frac{2}{\pi}\right)^{3/2} \frac{1}{k_i k_a^2} \left(\frac{E_a + c^2}{2E_a}\right) \sqrt{\frac{E_i + c^2}{2E_i}}$$

$$\times \sum_{\kappa_a m_a m_{la}} \sum_{\kappa_b m_b m_{lb}} \sum_{\kappa_i m_i m_{li}} \sum_{\lambda\rho} i^{(l_i - l_a - l_b)} e^{i(\delta^c_{k_a} + \delta^c_{k_b} + \eta_{k_a})} (-1)^{m_b - 1/2} \sqrt{2}(2j_a + 1)$$

$$\times (2j_b + 1)(2j_i + 1) \times \begin{pmatrix} l_a & 1/2 & j_a \\ m_{la} & s_a & -m_a \end{pmatrix} Y_{l_a m_{la}}(\hat{\vec{k}}_a) \times \begin{pmatrix} l_b & 1/2 & j_b \\ m_{lb} & s_b & -m_b \end{pmatrix} Y_{l_b m_{lb}}(\hat{\vec{k}}_b)$$

$$\times \begin{pmatrix} l_i & 1/2 & j_i \\ m_{li} & s_i & -m_i \end{pmatrix} Y^*_{l_i m_{li}}(\hat{\vec{k}}_i) \times \begin{pmatrix} j_b & \lambda & j_i \\ 1/2 & 0 & -1/2 \end{pmatrix} \begin{pmatrix} j_b & \lambda & j_i \\ -m_b & \rho & m_i \end{pmatrix}$$

$$\times \begin{pmatrix} 1/2 & \lambda & j_a \\ 1/2 & 0 & -1/2 \end{pmatrix} \begin{pmatrix} 1/2 & \lambda & j_a \\ -m_{1s} & \rho & m_a \end{pmatrix} \times T_R \quad (17)$$

For a specific case where the three spins are chosen, and with the 3j symbols providing one additional condition on the m values, we are left with two free m symmetries which are chosen to be m_{la} and m_{lb}.

In this work we let the kappa values κ_a, κ_b of the scattered electrons be the indices with infinite range. That leaves λ and κ_i for the incident electron to have a finite range. To

find the allowed value of λ we use the parity conditions and the triangle relations from the 3j symbols in equation (17).

From the 3j symbols (where the Helium bound state gave $\kappa = -1$, $l = 0$, and $j = 1/2$) we have the triangle inequalities

$$|j_a - 1/2| \leq \lambda \leq (j_a + 1/2) \tag{18}$$

$$|j_b - \lambda| \leq j_i \leq (j_b + \lambda) \tag{19}$$

with $l_a + \lambda$ and $l_b + \lambda + l_i$ even. From the first triangle inequality we get that $j_a = \lambda \pm 1/2$ and from the definition $l_a = j_a \pm 1/2$. Therefore we must have $\lambda = l_a$ and the two cases $j_a = l_a - 1/2$ and $\kappa_a = l_a$, or $j_a = l_a + 1/2$ and $\kappa_a = -l_a - 1$. Note that if $l_a = 0$ then we only have the case that $j_a = l_a + 1/2$.

2.2 Radial Part Of The Distorted Waves

The radial equations for the distorted waves, as given by [14], are

$$\left(\frac{d}{dr}+\frac{\kappa}{r}\right)f(r)-\alpha(E+\frac{1}{\alpha^2}-U(r))g(r)=\frac{\alpha}{r}W_Q(r) \tag{20}$$

$$\left(\frac{d}{dr}-\frac{\kappa}{r}\right)g(r)+\alpha(E-\frac{1}{\alpha^2}-U(r))f(r)=-\frac{\alpha}{r}W_P(r) \tag{21}$$

where $U(r)$ is the static potential of the atom in the initial channel, and the static potential of the ion in the final channel. α is the fine structure constant, and the W terms on the RHS of the equations are the exchange terms, which are given an explicit form and discussed in more detail in section 2.2.3.

2.2.1 Initial Channel

The solutions to the distorted waves in the initial channel follow [14] by writing the equations in integral form and using Simpson's rule to evaluate. The integral equations

are in the form

$$f(r) = v_{11}(r)\left[1 - \int_r^\infty (v_{12}(s)f(s) + v_{22}(s)g(s))U(s)ds\right] - v_{12}(r)\int_0^r ((v_{11}(s)f(s) + v_{21}(s)g(s))U(s)ds \quad (22)$$

$$g(r) = v_{21}(r)\left[1 - \int_r^\infty (v_{12}(s)f(s) + v_{22}(s)g(s))U(s)ds\right] - v_{22}(r)\int_0^r ((v_{11}(s)f(s) + v_{21}(s)g(s))U(s)ds \quad (23)$$

where v_{11}, v_{21} are the regular solutions, and v_{12}, v_{22} the irregular solutions of the radial Dirac equations with U = 0, and neglecting the W exchange terms for simplicity. In the initial channel U is the static potential of the neutral atom, which is a combination of the static potential of the nucleus and the bound electrons. Letting r_n be the radius of the nucleus, the static potential of the nucleus is given by $U_N(r) = -\frac{3Z}{2r_n} + \frac{Zr^2}{2r_n^3}$ for $r \leq r_n$, and $U_N(r) = -\frac{1}{r}$ otherwise (where $Z = 2$ for helium). The numerical solutions to the static potential of the electrons has been provided by Professor Robert McEachran and is evaluated from the expectation value of the potential of an electron.

These homogeneous solutions are constant multiples of the Ricatti-Bessel functions. More specifically they are given by

$$v_{11}(r) = \hat{j}_l(kr) \tag{24}$$

$$v_{12}(r) = -\alpha C_\alpha \hat{n}_l(kr) \tag{25}$$

$$v_{21}(r) = \frac{s_\kappa}{C_\alpha}\hat{j}_{\bar{l}}(kr) \tag{26}$$

$$v_{22}(r) = -\alpha s_\kappa \hat{n}_{\bar{l}}(kr) \tag{27}$$

where $\hat{j}_l$ and $\hat{n}_l$ are the Ricatti-Bessel functions (which are kr multiplied by the spherical Bessel functions) $s_\kappa = \frac{\kappa}{|\kappa|}$, $\bar{l} = l - s_\kappa$ and $C_\alpha = \frac{E+2c^2}{\sqrt{E(E+2c^2)}}$. Substituting these into equations (22) and (23) gives the integral equations

$$\begin{aligned} f(r) = \hat{j}_l(kr) - \alpha C_\alpha \hat{j}_l(kr) \\ \times \int_0^r (\hat{n}_l(ks)(f(s)U(s) - W_P(s)) + \frac{s_\kappa}{C_\alpha}\hat{n}_{\bar{l}}(ks)(g(s)U(s) + W_Q(s)))ds \\ + \alpha C_\alpha \hat{n}_l(kr) \int_0^r (\hat{j}_l(ks)(f(s)U(s) - W_P(s)) + \frac{s_\kappa}{C_\alpha}\hat{j}_{\bar{l}}(ks)(g(s)U(s) + W_Q(s)))ds \end{aligned} \tag{28}$$

$$g(r) = \frac{s_\kappa}{C_\alpha}\hat{j}_{\bar{l}}(kr) - \alpha s_\kappa \hat{j}_{\bar{l}}(kr)$$
$$\times \int_0^r (\hat{n}_l(ks)(f(s)U(s) - W_P(s)) + \frac{s_\kappa}{C_\alpha}\hat{n}_{\bar{l}}(ks)(g(s)U(s) + W_Q(s)))ds$$
$$+ \alpha s_\kappa \hat{n}_{\bar{l}}(kr) \int_0^r (\hat{j}_l(ks)(f(s)U(s) - W_P(s)) + \frac{s_\kappa}{C_\alpha}\hat{j}_{\bar{l}}(ks)(g(s)U(s) + W_Q(s)))ds \quad (29)$$

with the exchange terms W_P and W_Q retained and the factors of $\frac{1}{r}$ absorbed into them. Note also that the integrals from r to ∞ have been replaced with negative integrals from 0 to r.

Simpson's rule is then used to approximate the solutions with the subroutine BESJN from [17] used to compute the Bessel functions. In this work a different mesh is used than the one in [14] so that $h \to \frac{1}{\zeta'(r)} = dr$. Let the two integrals in f and g be represented as J(m) and I(m) respectively, then the equations f(m) and g(m) in the approximation are given by

$$f(m) = \Big((1 - \alpha C_\alpha J(m))\hat{j}_l(m) + \alpha C_\alpha I(m)\hat{n}_l(m)$$
$$- fac[(\frac{1}{C_\alpha} - \alpha J(m))s_\kappa \hat{j}_{\bar{l}}(m) + \alpha s_\kappa I(m)\hat{n}_{\bar{l}}(m)] + \frac{\alpha}{3\zeta'}(W_Q + fac \cdot W_P)\Big)/deta \quad (30)$$

$$g(m) = \Big(fac(1 - \alpha C_\alpha J(m))\hat{j}_l(m) + (\frac{1}{C_\alpha} - \alpha J(m)) s_\kappa \hat{j}_{\bar{l}}(m) \\ + (fac \cdot C_\alpha \hat{n}_l(m) + s_\kappa \hat{n}_{\bar{l}}(m)) I(m)\alpha + \frac{\alpha}{3\zeta'}(fac \cdot W_Q - W_P) \Big) / deta \quad (31)$$

with $fac = \frac{\alpha U_{atom}}{3\zeta'(m)}$, $deta = 1 + (fac)^2$, and U_{atom} as the static potential of the neutral atom. So U_{atom} becomes constant as $r \to 0$

2.2.2 Final Channel with Finite Nucleus Approximation

Starting with the differential equations of the distorted waves (Eqns (20), (21)) we let $U(r) = \frac{Z_n(r)}{r} + \bar{U}(r)$ in the final channel, with $Z_n(r) = -\frac{3r}{2r_n} + \frac{r^3}{2r_n^3}$ for $r < r_n$, and $Z_n(r) = -1$ otherwise, and where r_n is the radius of the nucleus. Now in the final channel, U(r) represents the static potential of the ion and we chose $Z_n(r)$ to be such that $\bar{U}(r) \to 0$ as $r \to \infty$, which allows the integral solutions to converge. To calculate the distorted waves in the final channel we put the equations in integral form. For the integral solutions, neglecting the exchange terms, we take

$$\begin{bmatrix} y_1 \\ y_2 \end{bmatrix} = \begin{bmatrix} f \\ g \end{bmatrix}, \quad A = \begin{bmatrix} -\frac{\kappa}{r} & (\alpha E + \frac{1}{\alpha} + Z_n(r)) \\ -(\alpha E - \frac{1}{\alpha} + \alpha Z_n(r)) & \frac{\kappa}{r} \end{bmatrix}, \quad \bar{c} = \begin{bmatrix} -\alpha \bar{U} y_2 \\ \alpha \bar{U} y_1 \end{bmatrix} \tag{32}$$

The homogeneous solutions are the solutions to $\bar{v}' = A\bar{v}$. These are the upper and lower

component functions

$$\begin{bmatrix} v_{11} \\ \\ v_{12} \end{bmatrix} = \begin{bmatrix} f_\kappa^{(u)}(kr) \\ \\ f_\kappa^{(l)}(kr) \end{bmatrix}, \quad \begin{bmatrix} v_{21} \\ \\ v_{22} \end{bmatrix} = \begin{bmatrix} g_\kappa^{(u)}(kr) \\ \\ g_\kappa^{(l)}(kr) \end{bmatrix} \tag{33}$$

which are calculated with the finite nucleus approximation. Using the homogeneous solutions in the same way they were used in the initial channel, the integral equations to $\bar{y}' = A\bar{y} + \bar{c}$ are then

$$y_1(r) = f_\kappa^{(u)}(kr) - \frac{\alpha}{\Delta} f_\kappa^{(u)}(kr) \int_0^r [g_\kappa^{(l)}(ks) y_2(s) + g_\kappa^{(u)}(ks) y_1(s)] \bar{U}(s) ds + \frac{\alpha}{\Delta} g_\kappa^{(u)}(kr) \int_0^r [f_\kappa^{(l)}(ks) y_2(s) + f_\kappa^{(u)}(ks) y_1(s)] \bar{U}(s) ds \tag{34}$$

$$y_2(r) = f_\kappa^{(l)}(kr) - \frac{\alpha}{\Delta} f_\kappa^{(l)}(kr) \int_0^r [g_\kappa^{(l)}(ks) y_2(s) + g_\kappa^{(u)}(ks) y_1(s)] \bar{U}(s) ds + \frac{\alpha}{\Delta} g_\kappa^{(l)}(kr) \int_0^r [f_\kappa^{(l)}(ks) y_2(s) + f_\kappa^{(u)}(ks) y_1(s)] \bar{U}(s) ds \tag{35}$$

where $\Delta = detV = f_\kappa^{(u)} g_\kappa^{(l)} - f_\kappa^{(l)} g_\kappa^{(u)}$. Note that the form of these equations including the exchange terms are given in Section 2.2.3 in equations (69) and (70). We can also

show that Δ is independent of r by looking at the equation $\bar{v}^{'} = A\bar{v}$. This gives

$$v_{x1}^{'}(r) = a(r)v_{x1}(r) + b(r)v_{x2}(r) \tag{36}$$

$$v_{x2}^{'}(r) = c(r)v_{x1}(r) + d(r)v_{x2}(r) \tag{37}$$

with a(r), b(r), c(r) and d(r) the components of the matrix A, prime denoting derivative with respect to r, and $v_{x1}(r) = f_{\kappa}^{(u)}$ or $g_{\kappa}^{(u)}$ and $v_{x2}(r) = f_{\kappa}^{(l)}$ or $g_{\kappa}^{(l)}$. Then we can substitute these equations into the derivative of Δ, which is given by

$$\Delta^{'} = f_{\kappa}^{(u)'} g_{\kappa}^{(l)} + f_{\kappa}^{(u)} g_{\kappa}^{(l)'} - f_{\kappa}^{(l)'} g_{\kappa}^{(u)} - f_{\kappa}^{(l)} g_{\kappa}^{(u)'} \tag{38}$$

To get

$$\Delta^{'} = [a(r) + d(r)]\Delta \tag{39}$$

but $a(r) = -\frac{\kappa}{r}$ and $d(r) = \frac{\kappa}{r}$ so that $\Delta^{'} = 0$. A specific value of Δ can be $\Delta = -\sqrt{\frac{E-c^2}{E+c^2}}$ by using the equations (166) and (170) in [17] (With E being the total energy including rest mass).

Using the Frobenius method the distorted waves and the Coulomb waves are calcu-

lated inside the nucleus. We then match the solutions around r_n by magnitude without matching slope. Matching both the upper and lower component solutions simultaneously results in a very small contribution from the irregular solutions. So the upper and lower solutions are matched separately.

In equations (34) and (35) we can call the two integrals from 0 to r, J(r) and I(r) respectively so that

$$I(r) = \int_0^r [f_\kappa^{(l)}(ks)y_2(s) + f_\kappa^{(u)}(ks)y_1(s)]\bar{U}(s)ds \tag{40}$$

$$J(r) = \int_0^r [g_\kappa^{(l)}(ks)y_2(s) + g_\kappa^{(u)}(ks)y_1(s)]\bar{U}(s)ds, \tag{41}$$

where $\bar{U}$ has Z=1 (in order to match the solutions of the full equation of U). So for $s < r_n$, $\bar{U}(s) = -\frac{3}{r_n} + \frac{c_o}{2} + \frac{s^2}{r_n^3} + O(s^3)$, where c_o is the constant term in the static potential of the bound electrons of helium and is equal to 3.3748629. The $\frac{1}{2}$ multiplied by c_o is due to the fact that in the final channel we now have a helium ion which has an electron in a state closer to that of the bound state of a hydrogen atom.

The Frobenius method solutions for the Coulomb waves and distorted waves for $\kappa < 0$

are

$$f_\kappa^{(u)}(s) = \sum_{i=0}^{n} a_{mc}(i) s^{2i+l+1}, \qquad f_\kappa^{(l)}(s) = \sum_{i=0}^{n} b_{mc}(i) s^{2i+l+2} \tag{42}$$

$$g_\kappa^{(u)}(s) = \sum_{i=0}^{n} a_{pc}(i) s^{2i-l}, \qquad g_\kappa^{(l)}(s) = \sum_{i=0}^{n} b_{pc}(i) s^{2i-l-1} \tag{43}$$

$$y_2(s) = \sum_{i=0}^{n} a_m(i) s^{2i+l+1}, \qquad y_1(s) = \sum_{i=0}^{n} b_m(i) s^{2i+l+2} \tag{44}$$

and for $\kappa > 0$

$$f_\kappa^{(u)}(s) = \sum_{i=0}^{n} a_{pc}(i) s^{2i+l+1}, \qquad f_\kappa^{(l)}(s) = \sum_{i=0}^{n} b_{pc}(i) s^{2i+l} \tag{45}$$

$$g_\kappa^{(u)}(s) = \sum_{i=0}^{n} a_{mc}(i) s^{2i-l}, \qquad g_\kappa^{(l)}(s) = \sum_{i=0}^{n} b_{mc}(i) s^{2i-l+1} \tag{46}$$

$$y_2(s) = \sum_{i=0}^{n} a_p(i) s^{2i+l+1}, \qquad y_1(s) = \sum_{i=0}^{n} b_p(i) s^{2i+l}, \tag{47}$$

where the value l in the equations corresponds to the respective value of κ. Plugging in

these Frobenius solutions into I(r) and J(r) and solving gives, for $\kappa < 0$,

$$I(r) = \int_0^r \left[\sum_{ij} a_{mc}(i) a_m(j) s^{2i+2j+2l+2} + \sum_{ij} b_{mc}(i) b_m(j) s^{2i+2j+2l+4} \right] (u_0 + u_2 s^2) ds$$
$$= \sum_{ij} \left[a_{mc}(i) a_m(j) \left(\frac{r^{2i+2j+2l+3}}{2i+2j+2l+3} u_0 + \frac{r^{2i+2j+2l+5}}{2i+2j+2l+5} u_2 \right) \right.$$
$$\left. + b_{mc}(i) b_m(j) \left(\frac{r^{2i+2j+2l+5}}{2i+2j+2l+5} u_0 + \frac{r^{2i+2j+2l+7}}{2i+2j+2l+7} u_2 \right) \right] \quad (48)$$

$$J(r) = \int_0^r \left[\sum_{ij} a_{pc}(i) a_m(j) s^{2i+2j+1} + \sum_{ij} b_{pc}(i) b_m(j) s^{2i+2j+1} \right] (u_0 + u_2 s^2) ds$$
$$= \sum_{ij} [a_{pc}(i) a_m(j) + b_{pc}(i) b_m(j)] \left(\frac{r^{2i+2j+2}}{2i+2j+2} u_0 + \frac{r^{2i+2j+4}}{2i+2j+2l+4} u_2 \right) \quad (49)$$

and for $\kappa > 0$

$$I(r) = \int_0^r \left[\sum_{ij} a_{pc}(i) a_p(j) s^{2i+2j+2l+2} + \sum_{ij} b_{pc}(i) b_p(j) s^{2i+2j+2l} \right] (u_0 + u_2 s^2) ds$$
$$= \sum_{ij} \left[a_{pc}(i) a_p(j) \left(\frac{r^{2i+2j+2l+3}}{2i+2j+2l+3} u_0 + \frac{r^{2i+2j+2l+5}}{2i+2j+2l+5} u_2 \right) \right.$$
$$\left. + b_{pc}(i) b_p(j) \left(\frac{r^{2i+2j+2l+1}}{2i+2j+2l+1} u_0 + \frac{r^{2i+2j+2l+3}}{2i+2j+2l+3} u_2 \right) \right] \quad (50)$$

$$J(r) = \int_0^r \left[\sum_{ij} a_{mc}(i) a_p(j) s^{2i+2j+1} + \sum_{ij} b_{mc}(i) b_p(j) s^{2i+2j+1} \right] (u_0 + u_2 s^2) ds$$

$$= \sum_{ij} [a_{mc}(i) a_p(j) + b_{mc}(i) b_p(j)] \left(\frac{r^{2i+2j+2}}{2i+2j+2} u_0 + \frac{r^{2i+2j+4}}{2i+2j+2l+4} u_2 \right), \quad (51)$$

where $u_0 = -\frac{3}{r_n} + \frac{c_0}{2}$ and $u_2 = \frac{1}{r_n^3}$. Combining each of the a and b coefficients in the Frobenius solutions allows us to simplify for matching and summing over κ. Let these combined coefficients be

$$a_{mm}(m) = \sum_{i=0}^{m} a_{mc}(\kappa, i) a_m(\kappa, m-i), \qquad b_{mm}(m) = \sum_{i=0}^{m} b_{mc}(\kappa, i) b_m(\kappa, m-i) \quad (52)$$

$$a_{pm}(m) = \sum_{i=0}^{m} a_{pc}(\kappa, i) a_m(\kappa, m-i), \qquad b_{pm}(m) = \sum_{i=0}^{m} b_{pc}(\kappa, i) b_m(\kappa, m-i) \quad (53)$$

$$a_{mp}(m) = \sum_{i=0}^{m} a_{mc}(\kappa, i) a_p(\kappa, m-i), \qquad b_{mp}(m) = \sum_{i=0}^{m} b_{mc}(\kappa, i) b_p(\kappa, m-i) \quad (54)$$

$$a_{pp}(m) = \sum_{i=0}^{m} a_{pc}(\kappa, i) a_p(\kappa, m-i), \qquad b_{pp}(m) = \sum_{i=0}^{m} b_{pc}(\kappa, i) b_p(\kappa, m-i). \quad (55)$$

Therefore, for $\kappa < 0$

$$I(r) = r^{2l+3} \sum_{m=0}^{n} [a_{mm}(m)u_0 + a_{mm}(m-1)u_2 + b_{mm}(m-1)u_0 + b_{mm}(m-2)u_2] \times \frac{r^{2m}}{2m+2l+3} \quad (56)$$

$$J(r) = r^2 \sum_{m=0}^{n} [a_{pm}(m)u_0 + a_{pm}(m-1)u_2 + b_{pm}(m)u_0 + b_{pm}(m-1)u_2] \frac{r^{2m}}{2m+2} \quad (57)$$

and for $\kappa > 0$

$$I(r) = r^{2l+1} \sum_{m=0}^{n} [a_{pp}(m-1)u_0 + a_{pp}(m-2)u_2 + b_{pp}(m)u_0 + b_{pp}(m-1)u_2] \times \frac{r^{2m}}{2m+2l+1} \quad (58)$$

$$J(r) = r^2 \sum_{m=0}^{n} [a_{mp}(m)u_0 + a_{mp}(m-1)u_2 + b_{mp}(m)u_0 + b_{mp}(m-1)u_2] \frac{r^{2m}}{2m+2} \quad (59)$$

2.2.3 Exchange Terms For The Distorted Waves

In the previous section the exchange terms in the distorted waves have been notated by W_Q and W_P. These terms appear in the differential equation for the distorted waves with a $\frac{1}{r}$ term in front and have the form

$$\frac{1}{r}W_{(P,\ Q)} = \Gamma_{J\mu J'}\frac{1}{r}Y_\mu(n^{'},\kappa^{'},\kappa,r)\,(P_{n'\kappa'}(r),\ Q_{n'\kappa'}(r)) \tag{60}$$

with

$$\frac{1}{r}Y_\mu(n^{'},\kappa^{'},\kappa,r) = \frac{1}{r^{\mu+1}}\int_0^r [P_{n'\kappa'}(s)y_1(s) + Q_{n'\kappa'}(s)y_2(s)]\,s^\mu ds + r^\mu\int_r^\infty [P_{n'\kappa'}(s)y_1(s) + Q_{n'\kappa'}(s)y_2(s)]\,\frac{ds}{s^{\mu+1}} \tag{61}$$

Specifically for the ground state $n^{'}\kappa^{'} = 1s$ so for $r \to 0$ we can let $P_{1s}(r) = pr$, $Q_{1s}(r) = qr^2$, $y_1(r) = ar^{l+1}$, and $y_2(r) = br^{\bar{l}+1}$ with $\mu = l$, with p, q, a, and b constants.

We can evaluate the four parts of the integrals;

$$\int_0^{r_2} \frac{P_{1s}(s)y_1(s)}{s^{\mu+1}}ds = pa\frac{r_2^2}{2} = \frac{P_{1s}(2)}{2}\frac{y_1(2)}{r_2^l} \tag{62}$$

$$\int_0^{r_2} \frac{Q_{1s}(s)y_2(s)}{s^{\mu+1}}ds = \begin{cases} qb\frac{r_2^2}{2} = \frac{Q_{1s}(2)}{2}\frac{y_2(2)}{r_2^l}, \kappa > 0 \\ qb\frac{r_2^4}{4} = \frac{Q_{1s}(2)}{4}\frac{y_2(2)}{r_2^l}, \kappa < 0 \end{cases} \tag{63}$$

$$\int_0^{r_2} s^{\mu}P_{1s}(s)y_1(s)ds = \frac{P_{1s}(2)}{2l+3}y_1(2)r_2^{l+1} \tag{64}$$

$$\int_0^{r_2} s^{\mu}Q_{1s}(s)y_2(s)ds = \begin{cases} \frac{Q_{1s}(2)}{2l+3}y_2(2)r_2^{l+1}, \kappa > 0 \\ \frac{Q_{1s}(2)}{2l+5}y_2(2)r_2^{l+1}, \kappa < 0 \end{cases} \tag{65}$$

The $\Gamma_{J\mu J'}$ in equation (60) is given by

$$\Gamma_{J\mu J'} = \begin{pmatrix} J & \mu & J' \\ \\ -1/2 & 0 & 1/2 \end{pmatrix}^2 \tag{66}$$

with the parity condition that $l+\mu+l'$ is even. For the ground state $n'\kappa' = 1s$ we have $\kappa' = -1 \Rightarrow l' = 0, \Rightarrow J' = 1/2$. By parity $\mu = l = J \pm 1/2$ so for $\kappa > 0$ we get $\mu = \kappa$ and for $\kappa < 0$ we get $\mu = -\kappa - 1$.

Evaluating Γ in the two regions gives

$$\Gamma_{J\mu J'} = \begin{cases} \frac{1}{2(2\kappa+1)}, & \kappa > 0 \\ \\ \frac{-1}{2(2\kappa+1)}, & \kappa < 0 \end{cases} \tag{67}$$

To include the exchange terms in the final channel integral equations we start with the column vector $\bar{c}$, and add the $\frac{W_{(P,Q)}(r)}{r}$ terms.

$$\bar{c} = \alpha \begin{bmatrix} -\bar{U}(r)y_2(r) + \frac{W_Q(r)}{r} \\ \\ \bar{U}(r)y_1(r) - \frac{W_P(r)}{r} \end{bmatrix} \tag{68}$$

The integral equations are then

$$\begin{aligned} & y_1(r) = f_\kappa^{(u)}(kr) \\ & - \frac{\alpha}{\Delta} f_\kappa^{(u)}(kr) \int_0^r \left[g_\kappa^{(l)}(ks) \left(y_2(s)\bar{U}(s) - \frac{W_Q(s)}{s} \right) + g_\kappa^{(u)}(ks) \left(y_1(s)\bar{U}(s) - \frac{W_P(s)}{s} \right) \right] ds \\ & + \frac{\alpha}{\Delta} g_\kappa^{(u)}(kr) \int_0^r \left[f_\kappa^{(l)}(ks) \left(y_2(s)\bar{U}(s) - \frac{W_Q(s)}{s} \right) + f_\kappa^{(u)}(ks) \left(y_1(s)\bar{U}(s) - \frac{W_P(s)}{s} \right) \right] ds \end{aligned} \tag{69}$$

$$
\begin{aligned}
y_2(r) &= f_\kappa^{(l)}(kr) \\
&- \frac{\alpha}{\Delta} f_\kappa^{(l)}(kr) \int_0^r \left[g_\kappa^{(l)}(ks) \left(y_2(s)\bar{U}(s) - \frac{W_Q(s)}{s} \right) + g_\kappa^{(u)}(ks) \left(y_1(s)\bar{U}(s) - \frac{W_P(s)}{s} \right) \right] ds \\
&+ \frac{\alpha}{\Delta} g_\kappa^{(l)}(kr) \int_0^r \left[f_\kappa^{(l)}(ks) \left(y_2(s)\bar{U}(s) - \frac{W_Q(s)}{s} \right) + f_\kappa^{(u)}(ks) \left(y_1(s)\bar{U}(s) - \frac{W_P(s)}{s} \right) \right] ds
\end{aligned}
\tag{70}
$$

2.2.4 Asymptotic Expansions

For large r ($r > r_N$), the radial distorted waves are exposed to a Coulomb potential from the ion, where r_N is the distance at which the bound orbitals are taken to be zero. This implies that an integral over the electron coordinates is equal to the number of electrons for these values of r and also that the total potential, including the nuclear term, is zero for the neutral atom. The radial distorted waves are then asymptotically linear combinations of the upper and lower component Coulomb functions. These functions themselves can be expressed as linear combinations of the non relativistic Coulomb functions which we will call G_λ and F_λ. From [17] we get the relationship that

$$G_\lambda + iF_\lambda = y_\lambda(\eta, x)e^{i\theta_\lambda} \tag{71}$$

$$G_\lambda - iF_\lambda = y^*_\lambda(\eta, x)e^{-i\theta_\lambda} \tag{72}$$

where $\lambda = \sqrt{\kappa^2 - (\alpha Z)^2}$, $y_\lambda(\eta, x) = {}_2F_0(i\eta - \lambda, i\eta + \lambda + 1, (2ix)^{-1})$, $x = kr$, $\eta = \frac{Z}{\nu}$ (with ν given after equation (87)), and $\theta_\lambda = x - \lambda\pi/2 - \eta ln(2x) + arg(\Gamma(\lambda + 1 + i\eta))$. Note that because the Dirac-Coulomb functions involve regular Coulomb functions with

non-integer parameters, both the regular and irregular solutions can be calculated from the power series of the confluent hypergeometric function, although in the case of the irregular solution a multiple of the regular solution must be added in order to get the correct asymptotic form.

Reference [17] contains a derivation of the asymptotic form of the Coulomb functions, and details of the coefficients and phase shifts of this asymptotic form.

In the asymptotic region, the distorted waves are

$$y_1 = AN[aF_\lambda(\eta, x) + bF_{\lambda-1}(\eta, x)] + BN[aG_\lambda(\eta, x) + bG_{\lambda-1}(\eta, x)] \tag{73}$$

$$y_2 = -AN[cF_\lambda(\eta, x) + dF_{\lambda-1}(\eta, x)] - BN[cG_\lambda(\eta, x) + dG_{\lambda-1}(\eta, x)] \tag{74}$$

where $A = 1 - \frac{\alpha}{\Delta} J(r_N)$, $B = \frac{\alpha}{\Delta} I(r_N)$, and $\Delta = -\sqrt{\frac{E-c^2}{E+c^2}}$, with I and J being the integrals from the section on the final channel distorted waves and E being the relativistic energy including rest mass. Recall also that the bound states $P_{1s}(r)$ and $Q_{1s}(r)$ are zero when $r > r_N$. The coefficients Na, Nb, -Nc, and -Nd are given in the subroutine DFASO from [17] which has been modified to produce the coefficients of ${}_2F_0$ (the hypergeometric

function).

Using equations (71) and (72) we can write these equations in a form better suited for contour integration;

$$y_1 = \frac{Na}{2}(B - iA)y_\lambda(\eta, x)e^{i\theta_\lambda} + \frac{Na}{2}(B + iA)y^*_\lambda(\eta, x)e^{-i\theta_\lambda} + \frac{Nb}{2}(B - iA)y_{\lambda-1}(\eta, x)e^{i\theta_{\lambda-1}} + \frac{Nb}{2}(B + iA)y^*_{\lambda-1}(\eta, x)e^{-i\theta_{\lambda-1}} \quad (75)$$

$$y_2 = -\frac{Nc}{2}(B - iA)y_\lambda(\eta, x)e^{i\theta_\lambda} - \frac{Nc}{2}(B + iA)y^*_\lambda(\eta, x)e^{-i\theta_\lambda} - \frac{Nd}{2}(B - iA)y_{\lambda-1}(\eta, x)e^{i\theta_{\lambda-1}} - \frac{Nd}{2}(B + iA)y^*_{\lambda-1}(\eta, x)e^{-i\theta_{\lambda-1}} \quad (76)$$

The two terms on each line of y_1 and y_2 are complex conjugates of each other. This implies that on the real axis the two distorted waves are just the real part of the first term on each line. To evaluate the asymptotic T-Matrix, contour integration is used separately on each term as different contours are needed.

In the incident channel the asymptotic distorted waves can be expressed as a linear combination of the Riccati-Bessel functions, and the Bessel functions can be expanded in

terms of the spherical Hankel functions

$$\hat{j}_l(kr) = \frac{h_l^+(kr) - h_l^-(kr)}{2i} = \frac{H_l^+(kr)e^{ikr} - H_l^-(kr)e^{-ikr}}{2i} \tag{77}$$

$$\hat{n}_l(kr) = \frac{h_l^+(kr) - h_l^-(kr)}{2} = \frac{H_l^+(kr)e^{ikr} - H_l^-(kr)e^{-ikr}}{2} \tag{78}$$

As before, asymptotically we have P_{1s}, $Q_{1s} = 0$ so then W_P, $W_Q = 0$ and $U_{atom} = 0$, which implies that $fac = 0$. Therefore we have the asymptotic expansion in the initial channel;

$$f_\kappa(r) \sim \left\{(1 - \alpha C_\alpha J(r_N))\frac{H_l^+(kr)}{2i} - \alpha C_\alpha I(r_N)\frac{H_l^+(kr)}{2}\right\} e^{ikr} - \left\{(1 - \alpha C_\alpha J(r_N))\frac{H_l^-(kr)}{2i} + \alpha C_\alpha I(r_N)\frac{H_l^-(kr)}{2}\right\} e^{-ikr} \tag{79}$$

$$g_\kappa(r) \sim \left\{(C_\alpha^{-1} - \alpha J(r_N))s_\kappa\frac{H_{\bar{l}}^+(kr)}{2i} - \alpha s_\kappa I(r_N)\frac{H_{\bar{l}}^+(kr)}{2}\right\} e^{ikr} - \left\{(C_\alpha^{-1} - \alpha J(r_N))s_\kappa\frac{H_{\bar{l}}^-(kr)}{2i} + \alpha s_\kappa I(r_N)\frac{H_{\bar{l}}^-(kr)}{2}\right\} e^{-ikr} \tag{80}$$

with $I(r_N)$ and $J(r_N)$ the integrals as defined in section 2.2.1, and C_α, s_κ also as defined in section 2.2.1.

2.2.5 Phase shifts and normalization

In the asymptotic region the distorted waves in the initial channel are a linear combination of the Riccati-Bessel functions, and in the final channel are a linear combination of the upper and lower component functions. If we call the coefficients of these linear combinations A_k and B_k such that, for example,

$$f_\kappa(r) = A_k \hat{j}_l(kr) + B_k \hat{n}_l(kr) \tag{81}$$

in the initial channel, and

$$y_1 = A_k f_\kappa^{(u)}(kr) + B_k g_\kappa^{(u)}(kr) \tag{82}$$

in the final channel, then the scattering phase shift is given by

$$tan(\delta_k^{sc}) = \frac{B_k}{A_k} \tag{83}$$

where these B and A have different values in the initial and final channel. The total

phase shift in the final channel involves a sum of this scattering phase shift and the Coulomb phase shift (see equations (86) and (87)). More specifically, in the initial channel we have

$$B_k = -\alpha C_\alpha I(r_N), \qquad A_k = 1 - \alpha C_\alpha J(r_N) \tag{84}$$

and in the final channel

$$B_k = \frac{\alpha}{\Delta} I(r_N), \qquad A_k = 1 - \frac{\alpha}{\Delta} J(r_N) \tag{85}$$

The total phase difference between the distorted waves f and g in the initial channel is the scattering shift δ_k^{sc} plus an additional factor of $\frac{\pi}{2}$. The phase difference between y_1 and y_2 in the final channel has additional contributions and is given by

$$\Delta\theta = \delta_k^{sc} + \frac{\pi}{2} + ln(2kr) + CS \tag{86}$$

with $k = \frac{\sqrt{E(E+2c^2)}}{c}$, the Coulomb shift, or CS, given by

$$CS = \nu - (\lambda - l - 1)\frac{\pi}{2} + arg\Gamma(\lambda + i\eta) - S_{Z,\kappa}\pi \tag{87}$$

With $\nu = arg[\alpha Z(E + c^2) - i(\kappa + \lambda)kc]$ and with $S_{Z,\kappa} = 1$ if $Z < 0$ and $\kappa < 0$, and $= 0$ otherwise.

The distorted waves are normalized by dividing by a factor of $\sqrt{A_k^2 + B_k^2}$. This gives the larger solution an amplitude of one.

3 Results and Discussion

In this section the results of the complete cross sections summed over all spin contributions are presented, as well as discussion of the relativistic effects on the results. We also examine the convergence of the partial waves in section 3.1. The results in section 3.3 also include a post-collision interaction term (Ward-Macek) in order to observe its effects on the behaviour of the cross section.

The calculations in this work are all in atomic units, so the cross sections have units of $\frac{a_0^2}{sr^2 au}$ where a_0 is the Bohr radius ($0.529177 \times 10^{-10} m$), au is the unit of energy (27.2114 eV), and sr is units of steradians (where the two values of sr correspond to the two outgoing electrons). In the figures, the units of energy and all angles are given in electron volts (eV), and degrees (^{0}) respectively. In each figure showing the calculated cross section with respect to an angle theta, we define theta as half of the angle between the two outgoing electrons. Theta is also the angle between each outgoing electron and the axis of symmetry between them. In this work the angle of the incident electron is taken to be 90 degrees with respect to the plane containing the outgoing electrons, and without loss of generality, we assume the incident electron has spin up.

3.1 Convergence Of The Partial Waves

The following figures are to demonstrate the convergence of the partial waves after a certain value of kappa. Note that in this section the value of kappa is a maximum value for the summation over the orbital angular momentums of the outgoing electrons. In the calculation of the T-matrix we sum over all possible combinations of angular momentum, where we take the orbital angular momentum quantum numbers from zero to kappa. Figure 1 is for an incident electron energy of 10 eV and Figure 2 for the case with 35 eV. Although for higher energy we do not see convergence until higher values of kappa, the two figures shown are almost if not completely converged by kappa=15 and 17 respectively.

Both figures are for the case with spin up on the bound electron and both outgoing electrons, which is allowed non relativistically. Other spin cases can be seen in the figures of section 3.2 and have similar converging behaviour for values of kappa greater than or equal to 15.

In both figures the cross section is zero at angles 0 and 180 with peak values at 90 degrees. Since electrons are fermions, we would expect the cross section to be zero at theta=0 and 180 degrees when the spins and energies of the outgoing electrons are the

same.

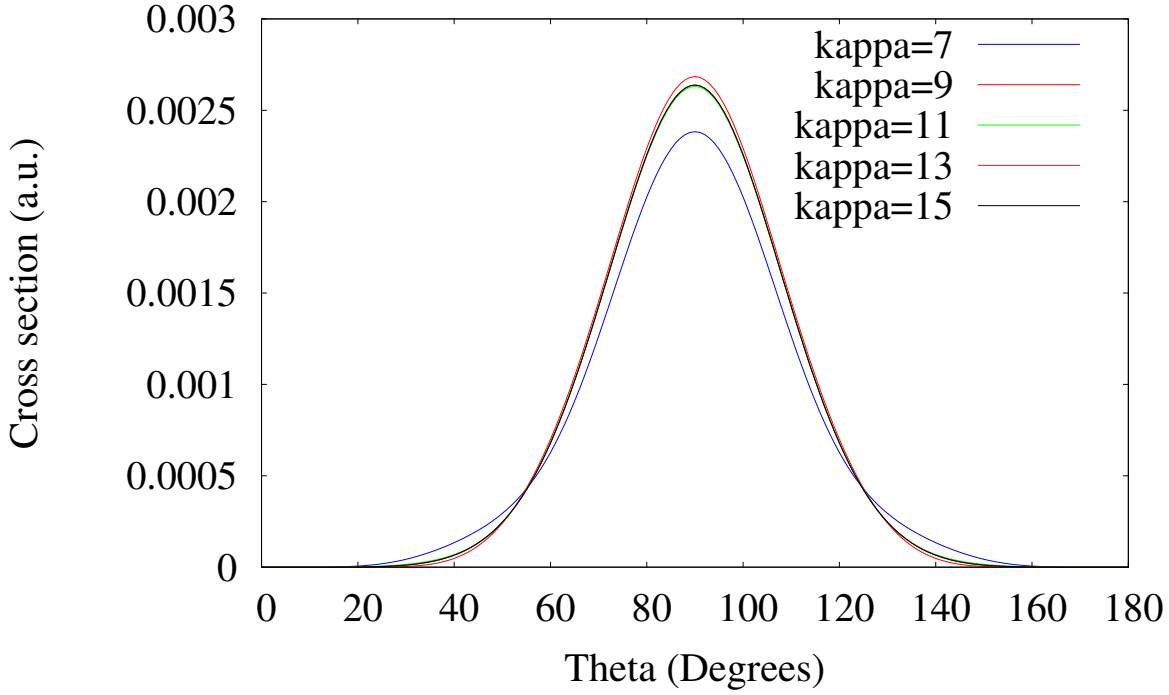

Figure 1: The cross section at 10 eV for the individual cases of kappa=7, 9, 11, 13, 15 with spin up for the bound electron and both outgoing electrons. We see complete convergence of the partial waves by kappa=15.

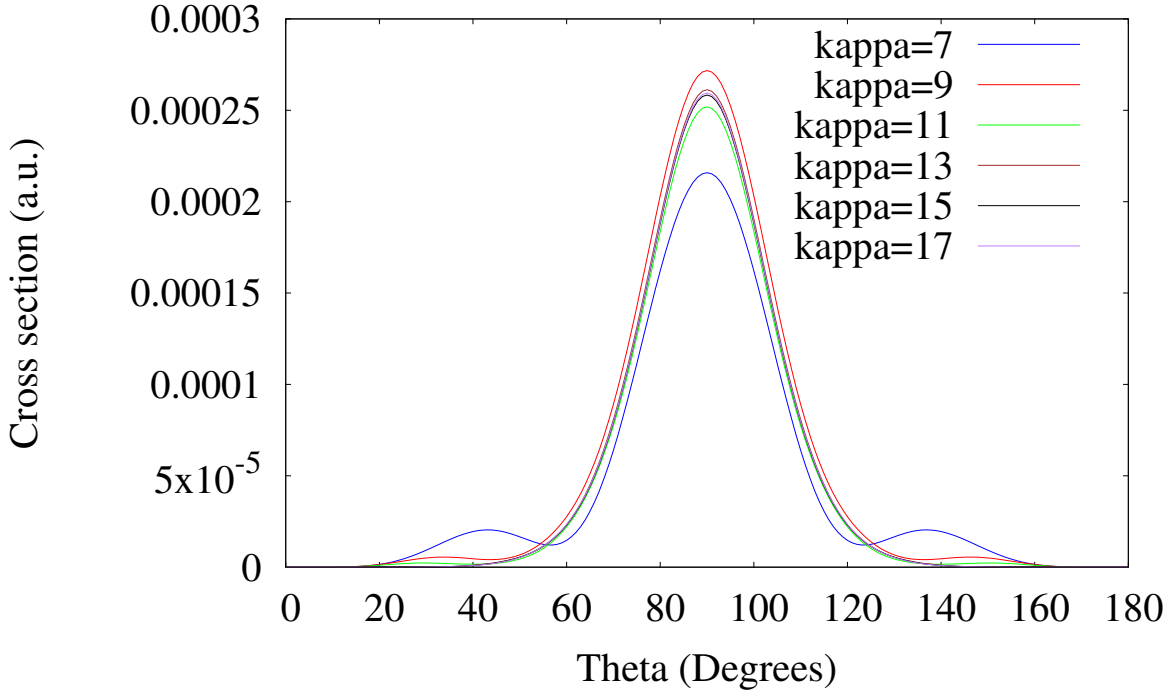

Figure 2: The cross section at 35 eV for the individual cases of kappa=7, 9, 11, 13, 15, 17. with spin up for the bound electron and both outgoing electrons. We see complete convergence of the partial waves by kappa=17.

3.2 Relativistic And Non Relativistic Spin Cases

Assuming the incident electron has spin up, we have eight possible cases for the spins of our total system. These cases come from the spin of the bound electron before it is ionized as well as the spins of the two outgoing electrons after the collision. Among these cases we can distinguish between what is allowed relativistically by observing whether or not the bound electron and incident electron have changed spin in the final channel. Since they are only allowed relativistically, the cases with one or more spin flip produce cross sections with a much lower magnitude.

The figures in the following pages are of the converged cross sections at 15 eV for three possible spin configurations of the total system. Figure 3 is possible non relativistically, while Figure 4 has the bound electron changing spin, and Figure 5 has both the bound electron and the incident electron changing spin in the final channel.

The general shape of the cross section for 15 eV, in the experimental results of [6], is a large central peak at 90 degrees with two smaller side peaks on either side. In the results of the individual spin cases presented here, we see a similar large central peak in the non

relativistically allowed figure 3. The cross section on either side of the central peak has small side peaks but does not go to zero at theta=0 and 180 degrees. This behaviour is not unexpected as the two outgoing spins are opposite which allows the electrons to occupy the same position.

A more notable difference is present in the relativistic cases in Figures 4 and 5. In Figure 4 we have almost the opposite behaviour, where we have zero cross section at 90 degrees, and larger side peaks. Figure 5 presents a central peak, but has a much more gradual decline in the cross section on either side approaching zero.

While the behaviour present in the relativistic cases seems like it may add certain features to the total cross section, note that the magnitudes in Figures 4 and 5 are much smaller. Figure 3 has a cross section around 10^{-2} where as Figures 4 and 5 are closer to 10^{-12} and 10^{-21} respectively. Even though five of the eight possible spin configurations are relativistic, the sum of the cross sections of all of these cases would still not be near the magnitude of the sum of the non relativistic cases. This relativistic contribution to the complete triple differential cross section would be very small and almost negligible for these results.

Since the helium nucleus has a very small charge it is not unexpected that the relativistic effects would also be small, since these effects depend on the total charge of the nucleus. It is interesting to note though, that in a similar collision with an atom that has a much greater charge on its nucleus (such as Xenon for example), the relativistic spin cases may make a much larger contribution to the complete cross section. This is something to be potentially looked at in a future work.

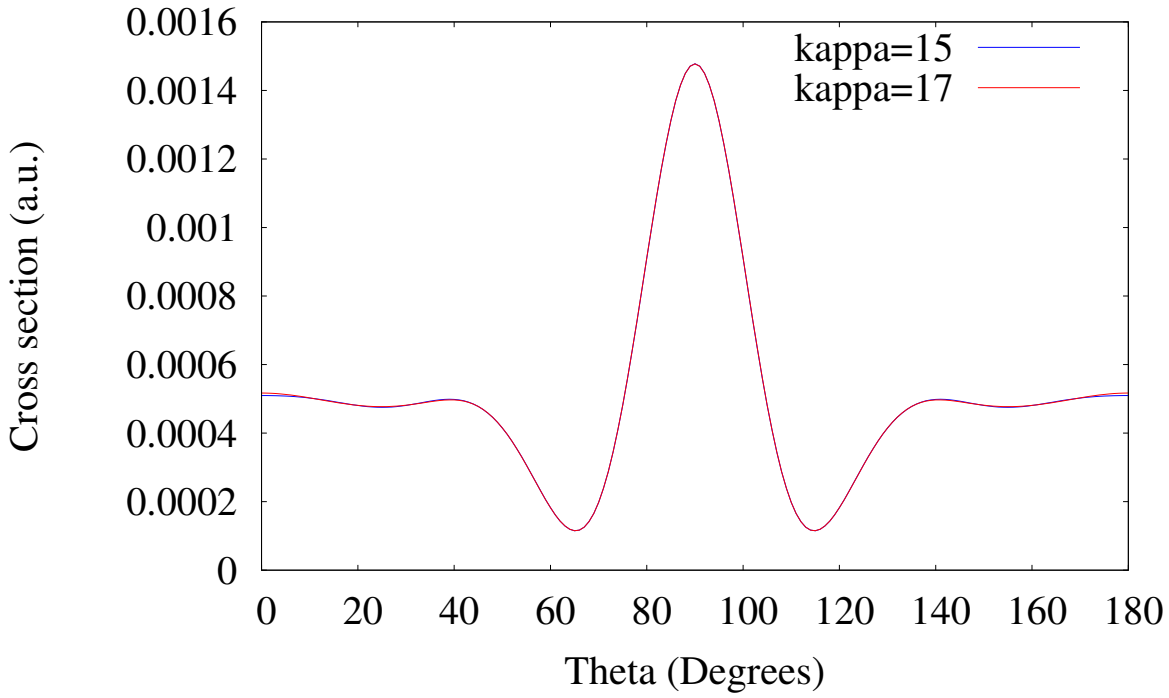

Figure 3: The cross section at 15 eV with spin down for the initially bound electron and one outgoing electron, and spin up for the other outgoing electron. This case is possible non relativistically and has non zero cross section at theta=0 and 180 degrees since the outgoing electrons have opposite spin. The partial waves of kappa=15 and 17 are shown to demonstrate convergence.

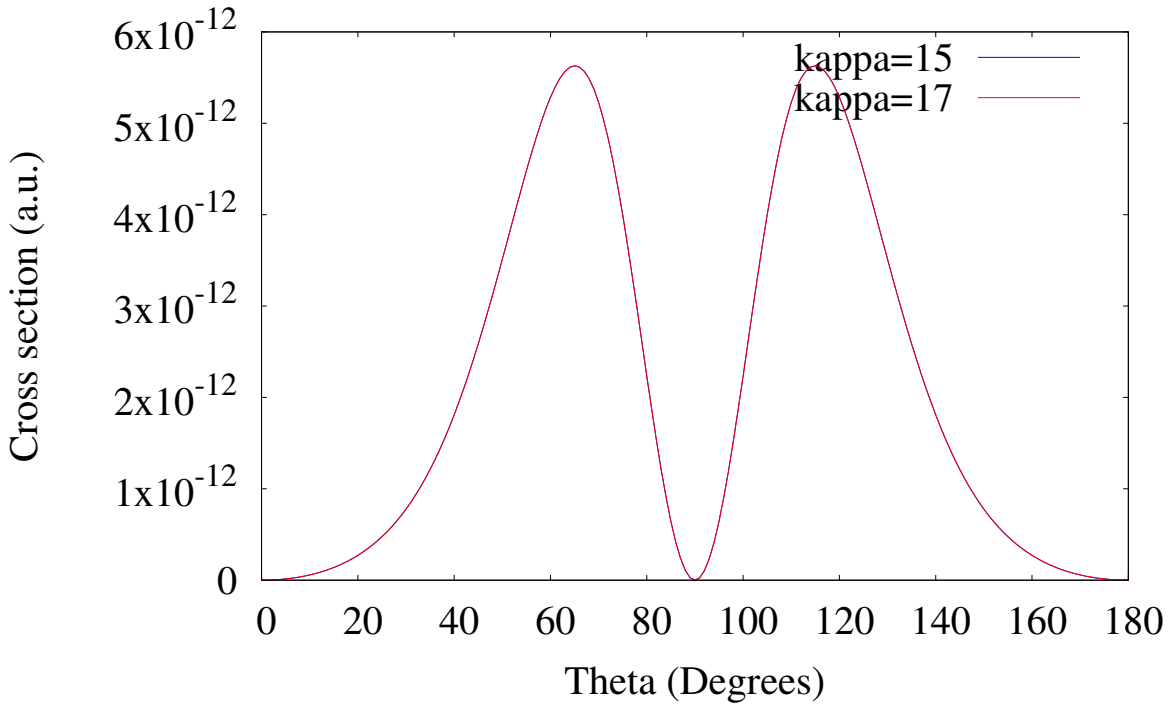

Figure 4: The cross section at 15 eV with spin down for the initially bound electron and spin up for both of the outgoing electrons. This case is only possible relativistically, as the bound electron has opposite spin in the final channel. The partial waves of kappa=15 and 17 are shown to demonstrate convergence.

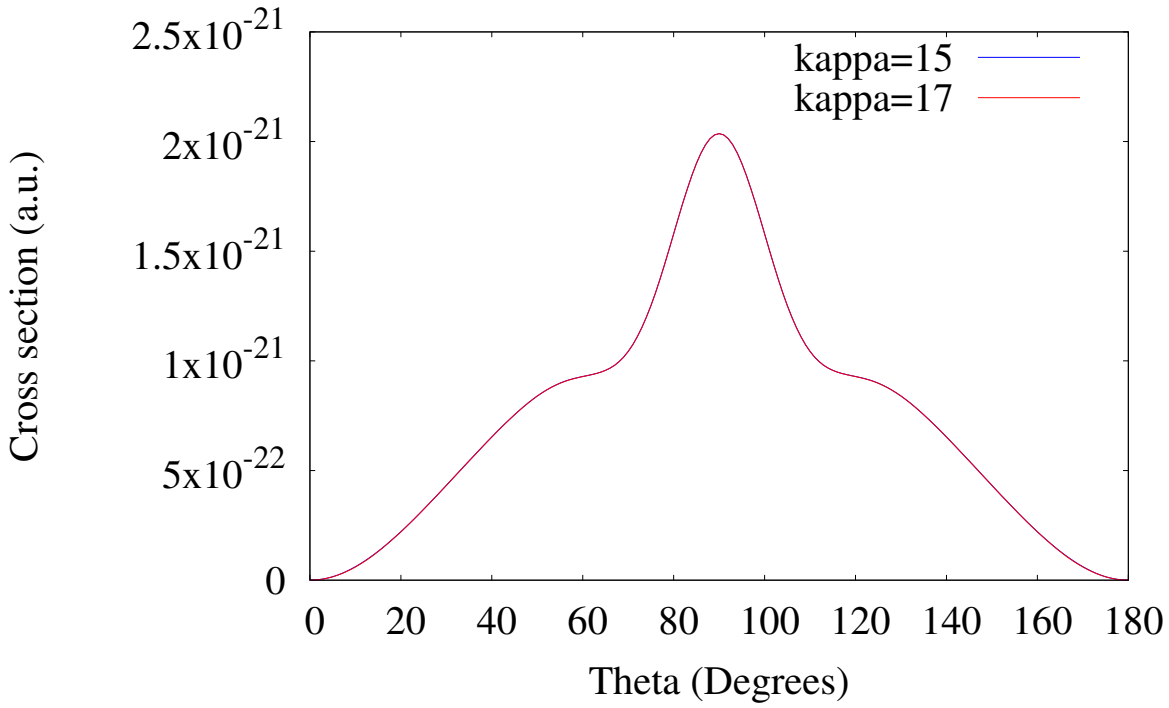

Figure 5: The cross section at 15 eV with spin up for the initially bound electron and spin down for both of the outgoing electrons. This case is only possible relativistically, as both the bound electron and incident electron have changed their spin in the final channel. The partial waves of kappa=15 and 17 are shown to demonstrate convergence.

3.3 Triple Differential Cross Sections And Experimental Results

The following pages contain the plots for the complete results of the cross section with and without the Ward-Macek factor, as well as results from [6] and experimental data from [4]. The results presented here from [6] do not include any post-collision interaction term (Ward-Macek or Gamow factors) as the effects of these terms are well understood.

Results for the Gamow factor are not shown as it has the same purpose as the Ward-Macek factor with differing magnitude. These differences in magnitude are not observed as each result is normalized at ninety degrees to the unmodified cross section (blue line) to allow the comparison of the shapes at all angles. Note that without this normalization the cross section results are still within the same magnitude as the results of [6].

The experimental error in the cross section is displayed at each point on the plots, while the experimental error in theta is constant at five degrees. The result for the plane wave approximation is only included in the lowest three energy plots, as it does not change shape significantly at higher energies.

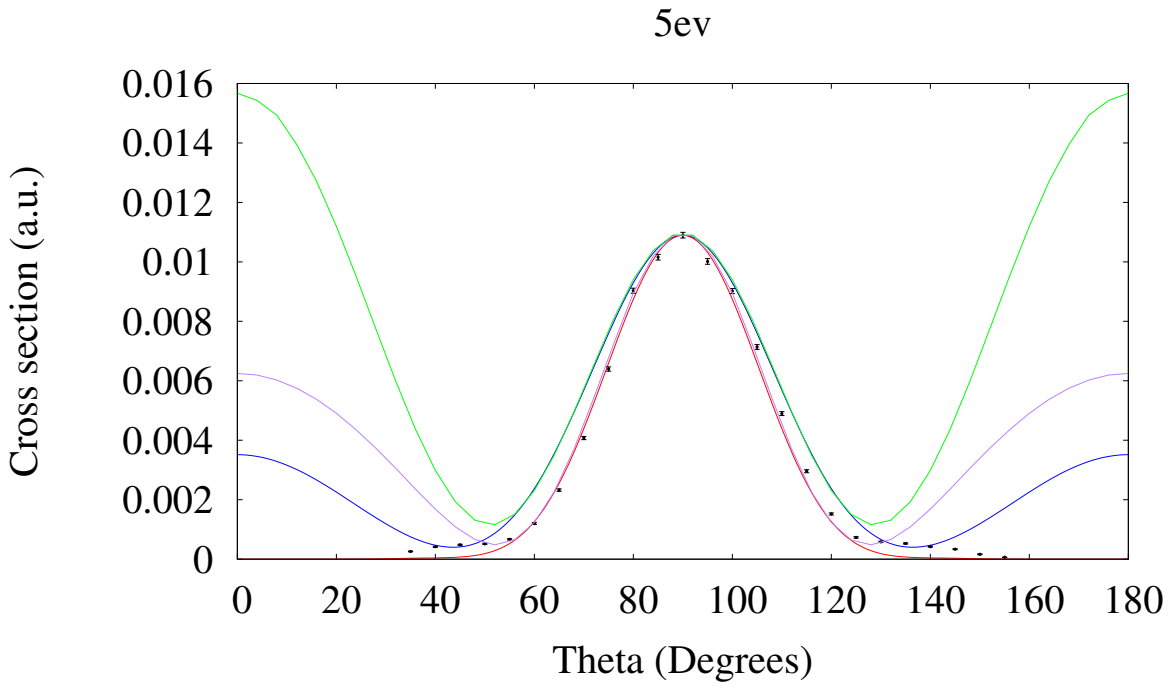

Figure 6: Triple differential cross sections for incident electron energy of 5 eV. Green line: plane wave approximation results of [6], purple line: distorted wave born approximation results of [6], blue line: present work without Ward-Macek, red line: present work including Ward-Macek, black points: experimental data from [4].

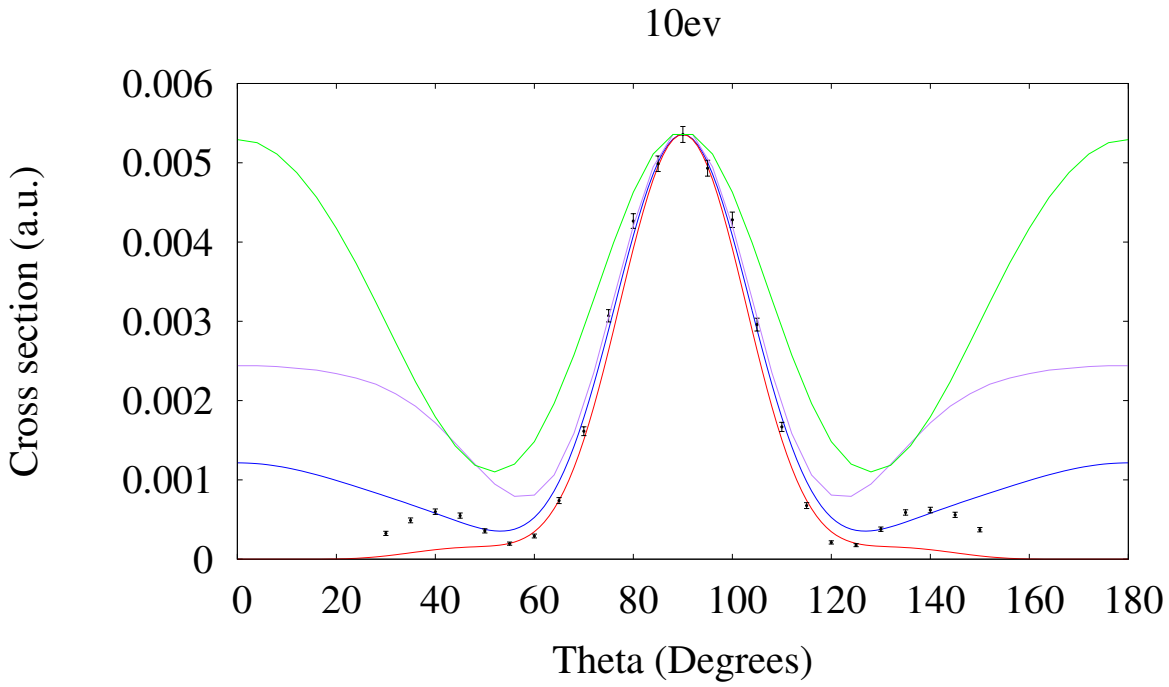

Figure 7: Triple differential cross sections for incident electron energy of 10 eV. Green line: plane wave approximation results of [6], purple line: distorted wave born approximation results of [6], blue line: present work without Ward-Macek, red line: present work including Ward-Macek, black points: experimental data from [4].

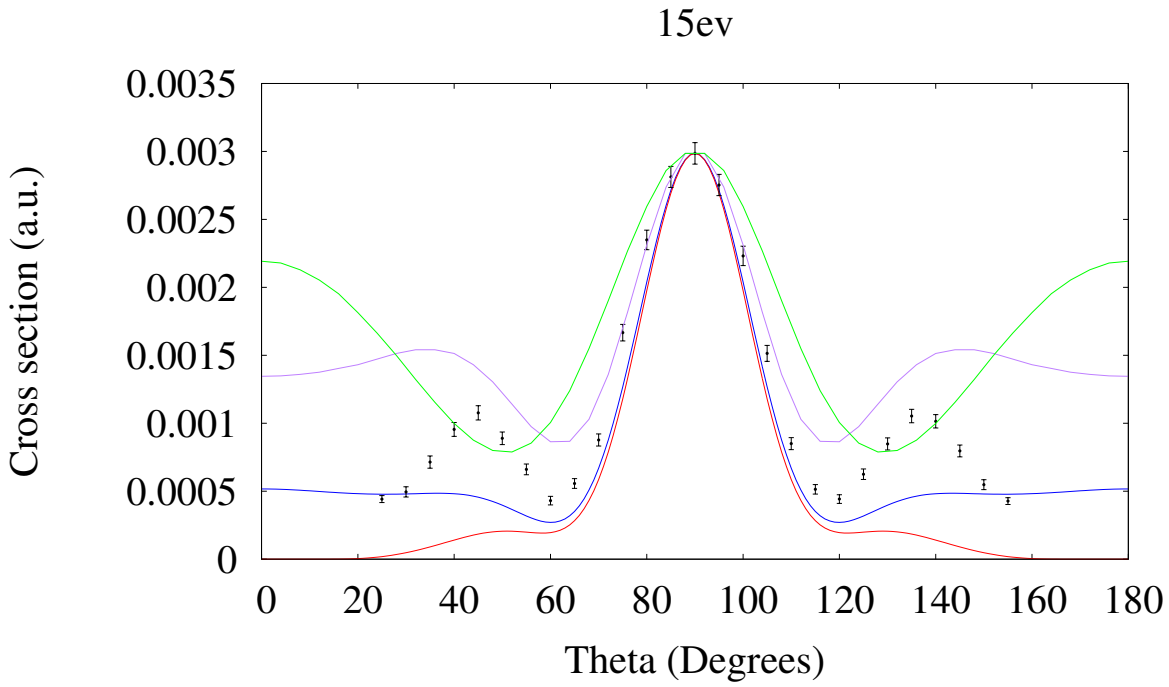

Figure 8: Triple differential cross sections for incident electron energy of 15 eV. Green line: plane wave approximation results of [6], purple line: distorted wave born approximation results of [6], blue line: present work without Ward-Macek, red line: present work including Ward-Macek, black points: experimental data from [4].

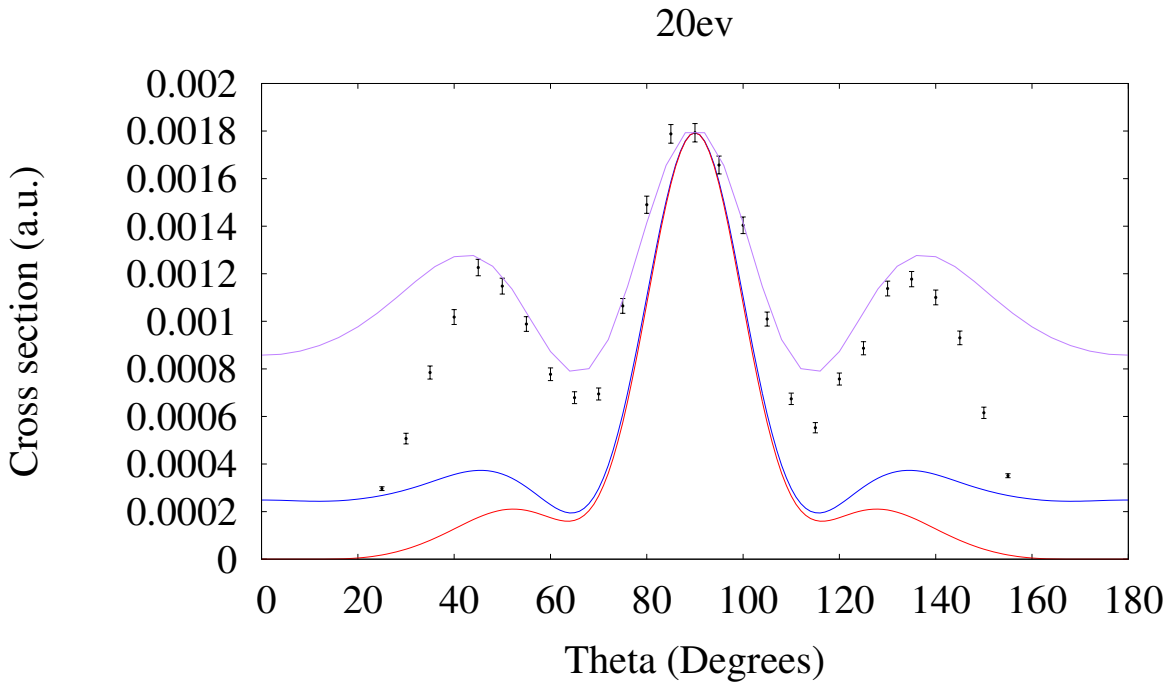

Figure 9: Triple differential cross sections for incident electron energy of 20 eV. Purple line: distorted wave born approximation results of [6], blue line: present work without Ward-Macek, red line: present work including Ward-Macek, black points: experimental data from [4].

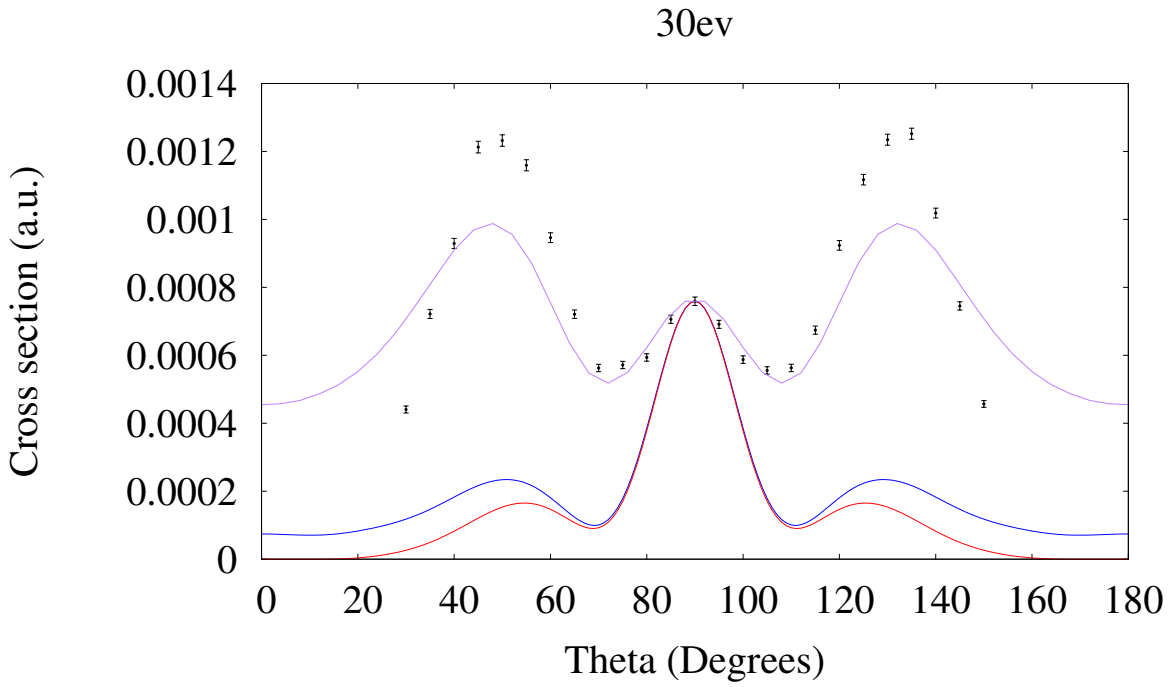

Figure 10: Triple differential cross sections for incident electron energy of 30 eV. Purple line: distorted wave born approximation results of [6], blue line: present work without Ward-Macek, red line: present work including Ward-Macek, black points: experimental data from [4].

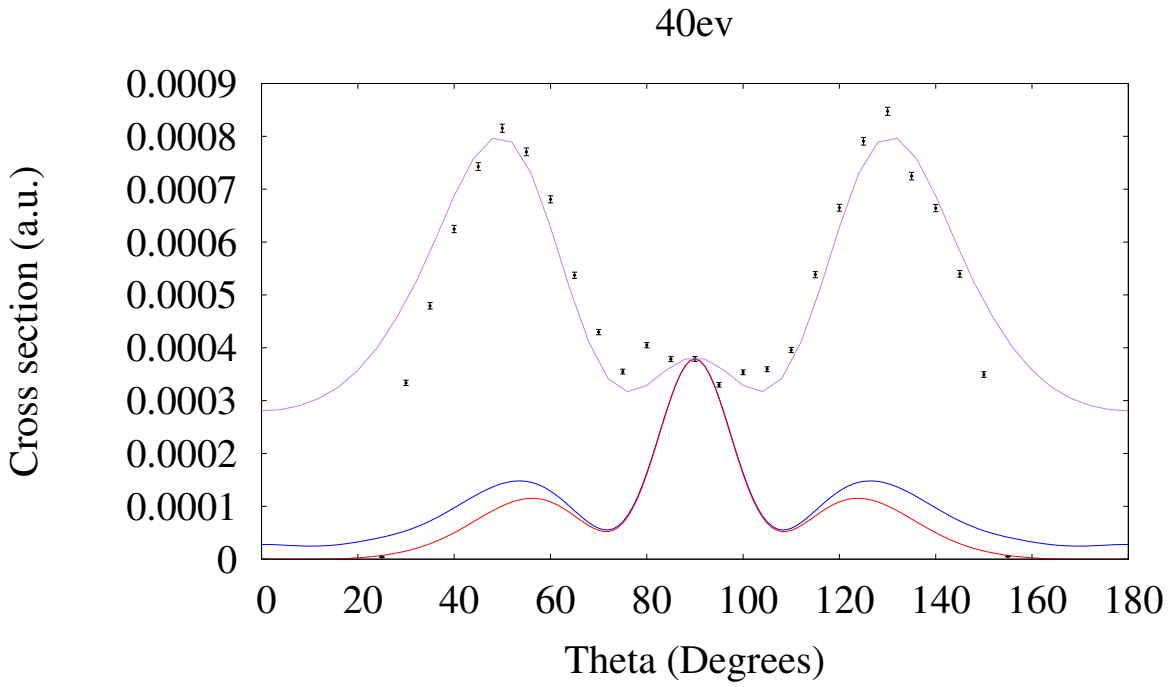

Figure 11: Triple differential cross sections for incident electron energy of 40 eV. Purple line: distorted wave born approximation results of [6], blue line: present work without Ward-Macek, red line: present work including Ward-Macek, black points: experimental data from [4].

3.3.1 Discussion

As we can see from the figures in the previous pages, the cross section with the Ward-Macek factor produces results that are comparable to the experimental data from [4] for lower energies, but lags behind in the magnitude of side peaks as the energy increases. The results of reference [6] are much better in this regard, but in some cases still does not produce side peaks of the same magnitude as the experimental results (most notably in the 30 eV case in figure 10). The width of the central peak also becomes wider as energy increases in the experimental results and the results of [6], whereas the cross section calculated in this work seems to have a constant width for the central peak, and as a result is less accurate for higher energies. Note that these cross sections were also calculated in the work of Zatsarinny and Bartschat [12], and produced similar results to that of Miller (reference [6]). In the lower three energy figures (Figures 6, 7, and 8) the plane wave approximation is also included. The plane wave approximation uses undistorted waves to calculate the T-matrix and therefore does not include the effect of the final waves scattering elastically from the ion. This causes a lack of side peaks in the plane wave results, which become more apparent at higher energies.

4 Conclusions and Further Work

There could be several reasons why there is an overall difference in shape between the results presented here and the results of reference [6]. In this work we used a full non-local exchange potential that arose from the antisymmetrization of the wave functions, whereas [6] used a local exchange which is a simpler calculation involving an additional term in the distortion potential. One would expect the non-local method to be more accurate, but it seems like the combination of distorted waves with a local potential might produce a better model of the ionization collision. Other differences between this work and [6] are the use of an integral equation method to solve for the distorted waves (as shown in section 2.2.1 and 2.2.2), and to get acceptable behaviour near the origin, a finite nucleus model was used.

It was also noted in Section 3.2 that the cross sections of the relativistic spin cases seemed to be the ones that had most of their behaviour away from ninety degrees. This behaviour away from the central peak in the experimental results from [4] is what differs most from the calculated results in this work, although it is not unexpected for the

relativistic results to be small as compared to the non relativistic cases, since the charge on the nucleus of helium is small.

As a further work, more promising results may be produced at smaller and larger theta if the inter electron interaction is explicitly included, as opposed to the use of the Ward-Macek or Gamow factor. Extending this work to heavier atoms would also allow for a more detailed look into the relativistic effects in these collisions, but the addition of electrons would increase the amount of exchange terms, and the non zero angular momentum of the outer shell would lead to extra terms from angular momentum coupling with the free waves. In order to produce the results in this work, programs were written that calculate the potentials, distorted waves, T-matrix, and cross sections. These programs can now be used to examine the use of these methods for other ionizations collisions such as the asymmetric co-planar configurations.

In conclusion, the results presented in this work were for a non coplanar ionization collision of a helium target in the case of the outgoing electrons having equal energy. The distorted waves were used as solutions to the relativistic Dirac equation with a non-local exchange, and calculated with the integral equation method. Direct and exchange T-matrix elements were used to calculated the cross sections for individual spin configu-

rations as well as for the total collision. The triple differential cross section was compared to the experimental results from reference [4] and the calculations from reference [6], and gave results comparable to experiment for lower energies, but became less accurate as energy increased.

Appendix A: T-Matrix With Asymptotic Correction

From Equation (13) in section 2.1.1, we evaluate the outer integral when $r_2 > r_N$ using the asymptotic correction method. The asymptotic expansions in section 2.2.4 can be written as

$$y_1(r) = Ce^{i(x-\eta ln(r))} + C^* e^{-i(x-\eta ln(r))} \tag{88}$$

$$y_2(r) = De^{i(x-\eta ln(r))} + D^* e^{-i(x-\eta ln(r))} \tag{89}$$

in the final channel, with $x = kr$, and

$$f_\kappa(r) = Ee^{ix'} + E^* e^{-ix'} \tag{90}$$

$$g_\kappa(r) = Fe^{ix'} + F^* e^{-ix'} \tag{91}$$

in the initial channel, where $x' = k'r$, $k' > k$, and (*) denotes complex conjugate in the

coefficients C, D, E, and F. Specifically these coefficients are given by

$$C = \frac{Na}{2}(B - iA)y_\lambda(\eta, x)e^{i(arg\Gamma(\lambda+1+i\eta)-\lambda\pi/2-\eta ln(2k))} + \frac{Nb}{2}(B - iA)y_{\lambda-1}(\eta, x)e^{i(arg\Gamma(\lambda+i\eta)-(\lambda-1)\pi/2-\eta ln(2k))} \quad (92)$$

$$D = -\frac{Nc}{2}(B - iA)y_\lambda(\eta, x)e^{i(arg\Gamma(\lambda+1+i\eta)-\lambda\pi/2-\eta ln(2k))} - \frac{Nd}{2}(B - iA)y_{\lambda-1}(\eta, x)e^{i(arg\Gamma(\lambda+i\eta)-(\lambda-1)\pi/2-\eta ln(2k))} \quad (93)$$

$$E = -\left[\alpha C_\alpha I(r_N) + i(1 - \alpha C_\alpha J(r_N))\right] H_l^+(kr)/2 \quad (94)$$

$$F = -\left[\alpha I(r_N) + i(C_\alpha^{-1} - \alpha J(r_N))\right] s_\kappa H_{\bar{l}}^+(kr)/2 \quad (95)$$

Thus the asymptotic part of the T-Matrix in equation (13) can be written as

$$\frac{y_1(r)f_\kappa(r)+y_2(r)g_\kappa(r)}{r^{\lambda+1}} = \frac{1}{r^{\lambda+1}}\Big\{ CEe^{i(x'+x-\eta ln(r))} + C^*Ee^{i(x'-x+\eta ln(r))} + CE^*e^{-i(x'-x+\eta ln(r))} + C^*E^*e^{-i(x'+x-\eta ln(r))} + DFe^{i(x'+x-\eta ln(r))} + D^*Fe^{i(x'-x+\eta ln(r))} + DF^*e^{-i(x'-x+\eta ln(r))} + D^*F^*e^{-i(x'+x-\eta ln(r))}\Big\}, \quad (96)$$

where the λ in this equation is the summation index as used in section 2.1.1, and the λ in equations (92) and (93) is the value as used in section 2.2.4. This λ as in equation (96) can be determined from the triangle inequalities and is equal to l_a in the direct term, and l_b in the exchange term.

Since the r dependant terms involve only inverse powers of r (other terms become constant as $r \to \infty$) there are no singularities for $r > r_N$. Therefore we can replace the integral on the real line by an integral along a line perpendicular to the real axis with contour integration.

In the first and third lines in the above equation the arguments of the exponentials

are positive, so we can use a contour integral in the first quadrant of the complex plane, starting at $R > r_1$ on the real line. This contour consists of the real axis for $r \geq R$, part of the circle at infinity, and the line perpendicular to the real axis given by $z = R + iy$, $y \geq 0$. Since there are no singularities inside the contour, and the integrand along the circle at infinity in the first quadrant vanishes exponentially, we can replace the integral along the real line by the integral along $z = R + iy$. Specifically;

$$\int_R^\infty \left[(CE + DF)e^{i(x' + x - \eta ln(r))} + (C^* E + D^* F)e^{i(x' - x + \eta ln(r))}\right] \frac{dr}{r^{\lambda+1}}$$
$$= -i \int_0^\infty \left[(CE + DF)e^{i(x' + x - \eta ln(r))} + (C^* E + D^* F)e^{i(x' - x + \eta ln(r))}\right] \frac{dy}{(R + iy)^{\lambda+1}} \quad (97)$$

where r is replaced by $R + iy$. Similarly the integral of the terms in the second and fourth lines of the full integrand equation can be replaced by a contour integral in the fourth quadrant of the complex plane that has the same form.

$$\int_R^\infty \left[(C^* E^* + D^* F^*)e^{-i(x' + x - \eta ln(r))} + (CE^* + DF^*)e^{-i(x' - x + \eta ln(r))}\right] \frac{dr}{r^{\lambda+1}}$$
$$= i \int_0^\infty \left[(C^* E^* + D^* F^*)e^{-i(x' + x - \eta ln(r))} + (CE^* + DF^*)e^{-i(x' - x + \eta ln(r))}\right] \frac{dy}{(R - iy)^{\lambda+1}} \quad (98)$$

where r is replaced by $R - iy$.

The two integrals above (including the factors of i in front) are complex conjugates of one another. Thus the total integral along the real line is just two times the real integral in the first quadrant. Since this integral is over the range $[0, \infty)$ and has a factor $e^{-(k^{'}+k)y}$, we use Gauss - Laguerre quadratures to evaluate it.

Consider the term

$$\int_R^\infty \left[(CE + DF) e^{i(x^{'}+x-\eta ln(r))} \right] \frac{dy}{(R+iy)^{\lambda+1}} \tag{99}$$

Using contour integration this can be put into the form

$$-i \int_0^\infty \left[C(R + \frac{iz}{k+k'}) E(R + \frac{iz}{k+k'}) + D(R + \frac{iz}{k+k'}) F(R + \frac{iz}{k+k'}) \right] \times e^{-i\eta ln(R + \frac{iz}{k+k'})} e^{i(k+k^{'})R} \frac{e^{-z}}{(R + \frac{iz}{k+k'})^{\lambda+1}} \frac{dz}{k+k'} \tag{100}$$

where $z = (k + k^{'})y$. Note that this is the first of two terms from the contour integral in the first quadrant (as in equation (97)), and the second term would have $z = (k^{'} - k)y$. Using Gauss-Laguerre quadrature, with z_m and w_m the Gauss-Laguerre roots and weights,

this integral is written as

$$-\frac{ie^{i(k+k^{'})R}}{k+k^{'}}\sum w_m f(z_m) \tag{101}$$

where $f(z)$ is the z-dependant terms in the integral without the e^{-z} which is included in the Gauss-Laguerre scheme.

Expanding the coefficients C, E, D, and F by writing

$$C(r) = C_1 y_\lambda(\eta, kr) + C_2 y_{\lambda-1}(\eta, kr) \tag{102}$$

$$E(r) = E_0 H_l^+(k^{'}r) \tag{103}$$

with

$$C_1 = Na\frac{(B-iA)}{2}e^{i(arg\Gamma(\lambda+1+i\eta)-\lambda\pi/2-\eta ln(2k))} \tag{104}$$

$$C_2 = Nb\frac{(B-iA)}{2}e^{i(arg\Gamma(\lambda+i\eta)-(\lambda-1)\pi/2-\eta ln(2k))} \tag{105}$$

$$E_0 = -\frac{1}{2}\left[\alpha C_\alpha I(R) + i(1-\alpha C_\alpha J(R))\right] \tag{106}$$

and similarly

$$D(r) = D_1 y_\lambda(\eta, kr) + D_2 y_{\lambda-1}(\eta, kr) \tag{107}$$

$$F(r) = F_0 H_{\bar{l}}^{+}(k^{'} r) \tag{108}$$

where

$$D_1 = -Nc\frac{(B - iA)}{2} e^{i(arg\Gamma(\lambda+1+i\eta)-\lambda\pi/2-\eta ln(2k))} \tag{109}$$

$$D_2 = -Nd\frac{(B - iA)}{2} e^{i(arg\Gamma(\lambda+i\eta)-(\lambda-1)\pi/2-\eta ln(2k))} \tag{110}$$

$$F_0 = -\frac{s_\kappa}{2}\left[\alpha I(r_N) + i(C_\alpha^{-1} - \alpha J(r_N))\right] \tag{111}$$

we can write

$$f(z) = \left(\frac{B - iA}{2}\right)\Bigg\{\left[NaE_0 H_l^{+}(k^{'} r) - NcF_0 H_{\bar{l}}^{+}(k^{'} r)\right] \times e^{i(arg\Gamma(\lambda+1+i\eta)-\lambda\pi/2-\eta ln(2k))} y_\lambda(\eta, kr) + \left[NbE_0 H_l^{+}(k^{'} r) - NdF_0 H_{\bar{l}}^{+}(k^{'} r)\right] e^{i(arg\Gamma(\lambda+i\eta)-(\lambda-1)\pi/2-\eta ln(2k))} y_{\lambda-1}(\eta, kr)\Bigg\} e^{-i\eta lnr}\frac{dz}{r^{\lambda+1}} \tag{112}$$

where $r = R + \frac{iz}{k+k'}$.

References

[1] A. Lahmam-Bennani (1991). *Recent developments and new trends in (e,2e) and (e,3e) studies.* J. Phys. B: At. Mol. Opt. Phys. 24 2401-2442

[2] A.J. Dempster (1918). *A new Method of Positive Ray Analysis.* Phys. Rev. 11, 316

[3] K.L. Nixon, A.J. Murray (2012). *Mapping the xenon (e,2e) differential cross section from coplanar to perpendicular geometries.* PHYSICAL REVIEW A 85, 022716

[4] K.L Nixon, A.J. Murray C. Kaiser (2010). *Low energy (e,2e) studies of the noble gases in the perpendicular plane.* J. Phys. B: At. Mol. Opt. Phys. 43 085202

[5] K.L Nixon A.J. Murray (2011). *Differential Cross Sections for Ionization of Laser-Aligned Atoms by Electron Impact.* PRL 106, 123201

[6] Miller, F.K. et al (2015). *Energy-sharing (e,2e) collisions: Ionization of the inert gases in the perpendicular plane.* PHYSICAL REVIEW A 91, 012706

[7] A. Illarionov, A.D. Stauffer (2012). *Calculation of non-coplanar electron-impact ionization of xenon.* J. Phys. B: At. Mol. Opt. Phys. 45 225202

[8] A. Dorn, A. Elliott, X. Guo, J. Hurn, J. Lower, S. Mazevet, I.E. McCarthy, Y. Shen, E. Weigold (1997). *(e,2e) collisions on xenon with spin-polarized electrons.* J. Phys. B: At. Mol. Opt. Phys. 30 4097-4121

[9] M.A. Stevenson, L.R. Hargreaves, B. Lohman, I. Bray,, D.V. Fursa, K. Bartschat, A. Kheifets (2009). *Fully differential cross-section measurements for the electron-impact ionization of neon and xenon.* PHYSICAL REVIEW A 79, 012709

[10] S. Chen, R.P. McEachran, A.D. Stauffer (2008). *Ab initio optical potential for elastic electron and positron scattering from the heavy noble gases.* J. Phys. B: At. Mol. Opt. Phys. 41 025201

[11] A.T. Stelbovics, I. Bray, D.V. Fursa, K. Bartschat (2005). *Electron-impact ionization of helium for equal-energy-sharing kinematics.* PHYSICAL REVIEW A 71, 052716

[12] O. Zatsarinny, K. Bartschat (2013). *The B-spline R-matrix method for atomic processes: application to atomic structure, electron collisions and photoionization.* J. Phys. B: At. Mol. Opt. Phys. 46 112001

[13] S. J. Ward and J. H. Macek (1994). *Wave functions for continuum states of charged fragments.* Phys. Rev. A 49, 1049

[14] Tao Zuo (1991). *Relativistic distorted-wave calculation of electron impact excitation of xenon.* PhD thesis York university

[15] Nouredine Zettili (2009). *Quantum Mechanics: Concepts and Applications 2nd edition.* ISBN 987-0-470-02679-3

[16] J.J. Sakurai and Jim Napolitano (2011). *Modern Quantum Mechanics Second Edition.* ISBN 978-0-8053-8291-4

[17] Salvat, Francesc et al (2008) *RADIAL: a Fortran subroutine package for the solution of the radial Schrodinger and Dirac wave equations*